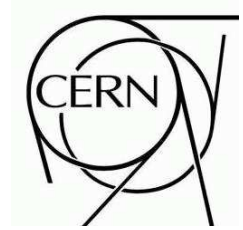




October 31, 2018



## Re-evaluation of the LHC potential for the measurement of $m_W$

Nathalie Besson, Maarten Boonekamp (CEA-Saclay),  
Esben Klinkby, Sascha Mehlhase, Troels Petersen (NBI)

### Abstract

We present a study of the LHC sensitivity to the  $W$  boson mass based on simulation studies. We find that both experimental and phenomenological sources of systematic uncertainties can be strongly constrained with  $Z$  measurements: the lineshape,  $d\sigma_Z/dm$ , is robustly predicted, and its analysis provides an accurate measurement of the detector resolution and absolute scale, while the differential cross-section analysis,  $d^2\sigma_Z/dydp_T$ , absorbs the strong interaction uncertainties. A sensitivity  $\delta m_W \sim 7$  MeV for each decay channel ( $W \rightarrow e\nu$ ,  $W \rightarrow \mu\nu$ ), and for an integrated luminosity of  $10 \text{ fb}^{-1}$ , appears as a reasonable goal.

# 1 Introduction

The Standard Model (SM), now computed at two-loop precision [1,2], is a very predictive framework. Its most precisely measured parameters  $\alpha_{QED}$ ,  $G_\mu$ , and  $m_Z$ , provide constraints on the  $W$  boson and top quark masses, which can be confronted with measurement. Injecting the measured value of the  $W$  mass and the measured  $Z$  boson couplings, a definite prediction is given for the top quark mass [3]. This prediction, together with the discovery of the top quark at a compatible mass [4,5], has been a major achievement in high energy physics.

The measured values of the  $W$  boson and top quark masses are now more precise than their quantum predictions, and provide non-trivial constraints on the gauge symmetry breaking sector. In the SM, this translates into limits on the Higgs boson mass [6]. Beyond the SM, constraints are given on the contributions of other heavy particles, like supersymmetric particles [7].

The  $W$  mass has been measured at UA2 [8], LEP [6], and the Tevatron [9]. The recent measurement by the CDF Collaboration gives  $m_W = 80.413 \pm 0.048$  GeV, yielding a current world average of  $m_W = 80.398 \pm 0.025$  GeV [10]. In the SM, the resulting Higgs boson mass uncertainty is about 50%. Any further improvement in this measurement will translate into more precise indirect predictions.

The present paper discusses the LHC prospects for the  $W$  mass measurement. The expected  $W$  cross-section at the LHC is about 20 nb [11]. In  $10 \text{ fb}^{-1}$  of data, a benchmark for one year of integrated luminosity during the first years of stable running, around  $4 \times 10^7$   $W$  events will be selected in each exploitable decay channel ( $W \rightarrow e\nu, \mu\nu$ ), providing a combined statistical sensitivity of about 1 MeV. Previous estimates [12–14] of the systematic uncertainties affecting this measurement however amount to  $\delta m_W \sim 20$  MeV per experiment, and to a combined uncertainty of  $\delta m_W \sim 15$  MeV. The main sources are the imperfect determination of the experiments absolute energy scale, and the uncertainties in the  $W$  boson kinematical distributions (rapidity, transverse momentum), which in turn stem from proton structure function uncertainties and higher orders QCD effects.

The purpose of this paper is to re-investigate the possibilities to measure the  $W$  mass with the greatest possible precision. As is known from the Tevatron, the uncertainties can be significantly reduced using  $Z$  boson measurements; this approach will be employed here, with modifications and improvements suggested by the high  $Z$  statistics expected. Although our discussion is general, most of our arguments rely on the expected performance of the ATLAS experiment [15].

The paper is structured as follows. Section 2 summarizes the  $W$  mass fitting procedure, lists the ingredients needed to describe the  $W$  distributions used in the fit, and gives a general description of how these ingredients can be determined. The sources of uncertainty are then discussed in turn, in Section 3 (experimental uncertainties), Section 4 (theoretical uncertainties), and Section 5 (backgrounds, underlying event, and effects related to the machine operation). Correlations between these effects are discussed in Section 6, and the results are given in Section 7. Section 8 concludes the paper.

## 2 General discussion

This section discusses our technical set-up, the  $W$  and  $Z$  event selection, the mass fitting procedure, and the problem of controlling all ingredients entering in the definition of the fitted distributions.

## 2.1 $W$ and $Z$ production. Event generation and simulation

Throughout this paper,  $W$  and  $Z$  boson samples, and their distributions and acceptances are computed using the PYTHIA general purpose event generator [16]. On top of PYTHIA, the treatment of photon radiation in  $W$  and  $Z$  decays is done via an interface to PHOTOS [17]. The size of the expected samples are computed assuming the NLO  $W$  and  $Z$  cross-sections, as obtained from RESBOS [18]. These choices are not unique, and the simulation of physics processes at the LHC, in particular non-perturbative strong interaction parameters, will obviously need to be adjusted using the forthcoming data. In this analysis, the effects of the corresponding uncertainties are estimated either by changing parameters in these programs, or by distorting the output distributions according to our assumptions.

When referring to “fast simulation”, we mean a simplified simulation of the ATLAS detector response using scale factors and Gaussian resolution functions, applied to the generator-level information obtained above [19]. When referring to “full simulation”, we mean the complete simulation of the ATLAS detector using GEANT4 [20]. In our discussions below, and in the absence of real physics data, we often treat our fully simulated event samples as data samples, and the fast simulation samples as their Monte-Carlo simulation. The different detector response in fast and full simulation allows to emulate the realistic situation where the imperfect detector simulation is adjusted during data taking.

## 2.2 Signal selection and fitting procedure

At hadron colliders,  $W$  and  $Z$  events can be detected and reconstructed in the  $e\nu_e$ ,  $\mu\nu_\mu$ ,  $ee$ , and  $\mu\mu$  final states. The hadronic modes suffer prohibitively large background from jet production;  $\tau$  modes can be detected but the  $\tau$ -lepton decay produces additional undetected particles in the final state, diluting the information that can be extracted from these modes. In  $W$  events, the observables most sensitive to  $m_W$  are:

- The reconstructed lepton transverse momentum,  $p_T^\ell$ ;
- The reconstructed  $W$  transverse mass,  $m_T^W \equiv \sqrt{2p_T^\ell p_T^\nu (1 - \cos(\phi^\ell - \phi^\nu))}$ .

The transverse momentum of the neutrino,  $p_T^\nu$ , is inferred from the transverse energy imbalance, calculated from a summation of energy in all calorimeter cells. Electrons are measured using the inner detector (ID) and electromagnetic calorimeter (EMC). They are reconstructed and identified with an efficiency of about 65%, while rejecting background from jets up to one part in  $10^5$ ; in  $W$  decays, the energy resolution is about 1.5%. For muons, the ID is used together with the muon spectrometer; the reconstruction efficiency is about 95% and the relative momentum resolution about 2% [21].

The  $W$  signal is extracted by selecting events with one reconstructed isolated, high- $p_T$  lepton (electron or muon), large missing transverse energy (due to the undetected neutrino), and low hadronic activity. In the following, we require  $p_T^\ell > 20$  GeV,  $|\eta_\ell| < 2.5$ ,  $E_T^{miss} > 20$  GeV, and require the hadronic recoil (defined as the vector sum of all calorimetric transverse energy opposite to the reconstructed  $W$  decay products) to be smaller than 30 GeV. These selections have a total efficiency (trigger and selection) of about 20%, providing a sample of about  $4 \times 10^7$  events in each decay channel. The backgrounds are at the percent level. Table 1 summarizes these numbers. The  $p_T^\ell$  and  $m_T^W$  distributions obtained with fast simulation after the  $W$  event selection are shown in Figure 1.

Based on these distributions,  $m_W$  can be extracted by comparing the data to a set of models (or template distributions) obtained from  $W$  event generation followed by a fast simulation of the decay particles.

Channel	$W \rightarrow l\nu$	$Z \rightarrow ll$
Cross-section (pb)	19800	1870
Lepton $\eta$ acceptance	0.63	0.51
Selection eff. (including acceptance)	$\sim 0.2$	$\sim 0.2$
Expected statistics ( $10 \text{ fb}^{-1}$ )	$4 \times 10^7$	$3.5 \times 10^6$

Table 1: Cross-section,  $\eta$  acceptance, total selection efficiency (averaged for electrons and muons) and expected sample size for  $10 \text{ fb}^{-1}$ , in each decay channel.

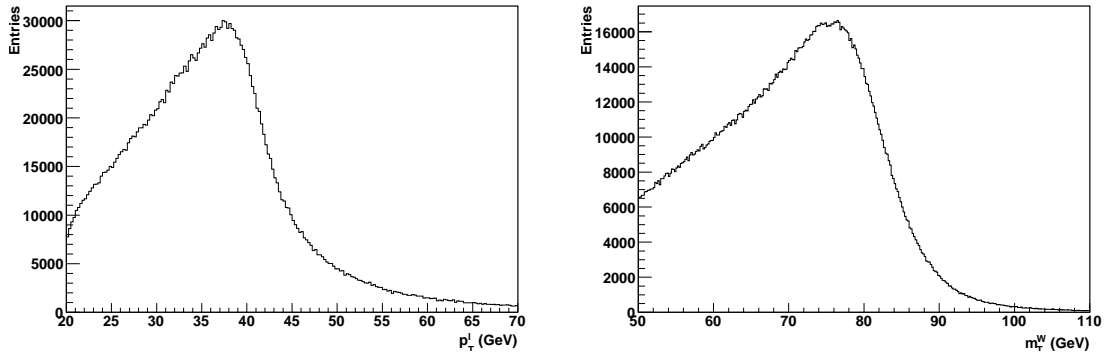


Figure 1: Distributions of the lepton transverse momentum,  $p_T^\ell$ , and of the  $W$  transverse mass,  $m_T^W$ , after typical  $W$  event selections (cf. text). The Jacobian edges in these distributions provide sensitivity to the  $W$  mass.

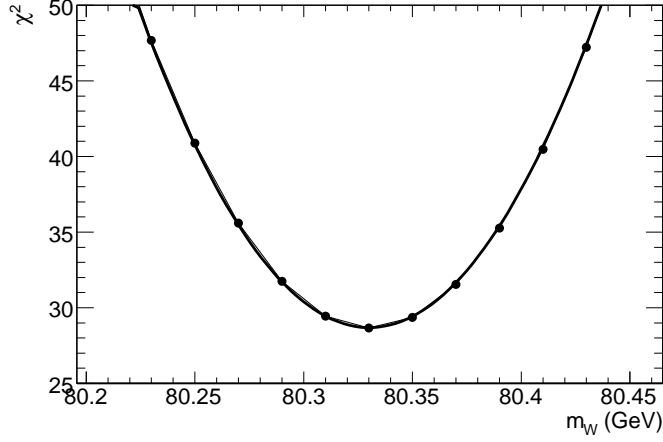


Figure 2:  $\chi^2$  value as function of the tested value of  $m_W$ . Each dot represents a comparison between the data and the template distribution obtained for a given  $m_W$ . The curve is the fitted parabola.

The different template distributions are obtained by varying the value of the  $W$  boson mass parameter in the event generation. The statistical comparison of the data to the templates can be performed in various ways; throughout this study we will use a simple binned  $\chi^2$  test. The  $\chi^2$  quantifying the compatibility of a given template distribution with the data is defined as follows:

$$\chi^2 = \sum_i \frac{(n_i^{obs} - n_i^{exp})^2}{\sigma_i^2} \quad (1)$$

where  $n_i^{exp}$  and  $n_i^{obs}$  are the number of expected and observed events (in the template distribution and in the data, respectively) in bin  $i$  of the  $p_T^\ell$  or  $m_T^W$  spectrum,  $\sigma_i$  is the expected resolution, and the sum extends over all bins in the fitting window. The Gaussian approximation used above is justified for large statistics, which is the case we consider here.

After all  $\chi^2$  evaluations, a parabola is fitted through the  $\chi^2$  values as a function of  $m_W$ . The procedure is illustrated in Figure 2. With the statistics given in Table 1, each channel provides a statistical precision of about 2 MeV for data corresponding to an integrated luminosity of  $10 \text{ fb}^{-1}$ .

### 2.3 Required inputs

For the above procedure to work in practice, one must predict the  $p_T^\ell$  and  $m_T^W$  distributions as a function of the  $W$  mass. These distributions are however affected by many effects, which need to be included correctly in order to avoid biases in the mass fit. The needed inputs are listed below.

- **Experimental inputs:** the energy scale and resolution need to be known in order to describe the Jacobian peak correctly (position and spread). Electron and muon reconstruction efficiency effects also distort the spectra, if this efficiency is  $p_T$  and  $\eta$  dependent.

- **Theoretical inputs:** the  $W$  rapidity distribution,  $y^W$ , affects the  $m_T^W$  and  $p_T^\ell$  distributions. The transverse momentum of the  $W$ ,  $p_T^W$ , directly affects the  $p_T^\ell$  spectrum; its impact is weaker on the  $m_T^W$  spectrum. The  $y^W$  and  $p_T^W$  distributions depend on the proton structure functions and on higher-order QCD effects. The lepton angular distribution in the  $W$  rest frame is of importance for both  $p_T^\ell$  and  $m_T^W$  and changes with the  $W$  polarization [22]. Finally, QED effects (photon radiation in the  $W$  decay) shifts the lepton  $p_T$  downwards. Since the radiated photons are mostly collinear to the charged decay lepton, the impact on electrons and muons is different: the measured muon momentum entirely reflects the momentum loss by radiation, whereas the electron energy, measured essentially in the EMC, includes most of the radiated energy.

- **Environmental inputs:** these include, among others, backgrounds surviving the  $W$  selection, underlying event and pile-up effects on reconstructed energies and momenta, random neutron hits in the muon spectrometer (“cavern background”), and the impact of a non-zero beam crossing angle. In all cases, imperfect modelling of these inputs biases the event reconstruction, leading to distorted  $p_T^\ell$  and  $m_T^W$  distributions.

## 2.4 Propagation of systematic uncertainties

The impact of underlying physics mechanisms affecting the  $W$  mass determination is estimated by producing template distributions of  $p_T^\ell$  and  $m_T^W$  unaware of the effect under consideration, and fitting them to pseudo-data including this effect. The resulting bias (i.e. the difference between the injected and fitted values of  $m_W$ ) gives the corresponding systematic uncertainty.

In the simplest case, a physics effect affecting the distributions (for a given value of the  $W$  mass) can be summarized by a single parameter. In this case, the induced systematic uncertainty is simply given by:

$$\delta m_W = \frac{\partial m_W}{\partial_{rel} \alpha} (\delta_{rel} \alpha) \quad (2)$$

where  $\alpha$  is the parameter controlling the parasitic physics effect,  $\delta_{rel} \alpha$  its relative uncertainty, and  $\delta m_W$  the induced systematic uncertainty on the  $W$  mass. When applicable, we will quote the uncertainty  $\delta_{rel} \alpha$ , the derivative  $\partial m_W / \partial_{rel} \alpha$  and the estimated  $\delta m_W$ . As a convention, we normalize  $\partial m_W / \partial_{rel} \alpha$  in MeV/%.

Sometimes, however, a single parameter is not sufficient. The uncertainty  $\delta m_W$  is then the result of all parameter uncertainties and their correlations:

$$\delta m_W^2 = \sum_{i,j} \frac{\partial m_W}{\partial_{rel} \alpha_i} \frac{\partial m_W}{\partial_{rel} \alpha_j} (\delta_{rel} \alpha_i) (\delta_{rel} \alpha_j) \rho_{ij}. \quad (3)$$

This happens when the systematic is parametrized by a (sometimes empirical) function. In this case, we choose to quantify the impact by Monte-Carlo propagation: we generate random configurations of the  $\alpha_i$ , within their uncertainties, and preserving their correlations; for each configuration, we produce the corresponding pseudo-data, and fit them to the unaffected templates. The spread of the distribution of the fitted  $m_W$  values gives the contribution to  $\delta m_W$ .

## 2.5 The impact of $Z$ boson measurements

The LHC will produce a large number of  $Z$  events. Their selection is rather straightforward, requiring two reconstructed isolated, high- $p_t$  leptons ( $p_T^\ell > 20$  GeV,  $|\eta_\ell| < 2.5$ ), and low hadronic activity (hadronic recoil smaller than 30 GeV).

For each useful decay mode ( $Z \rightarrow ee, \mu\mu$ ) and for  $\sim 10 \text{ fb}^{-1}$ , around  $3.5 \times 10^6$  events should survive selections. This represents a factor 10 less than the expected  $W$  statistics, but the fact that  $Z$  events are fully reconstructed largely compensates this deficit. Cross-sections and statistics are summarized in Table 1.

The precise knowledge of the  $Z$  mass and width will allow to determine the lepton energy scale and resolution precisely. Exploiting the energy distribution from the decay leptons will also allow to determine the scale's energy dependence (i.e., the linearity of the detector response), and the energy dependent resolution function. Once this is achieved, the  $Z$  transverse momentum will also serve to scale the measured hadronic recoil to the  $Z$ ; together with the measured lepton transverse momentum, this defines the missing transverse energy. Finally, “tag and probe” methods [23] will allow to determine the lepton reconstruction efficiency.

Although most of the QCD mechanisms affecting  $W$  distributions carry significant uncertainty [24], they affect  $W$  and  $Z$  events in a similar way. This is the case for non-perturbative contributions to the  $W$  transverse momentum distributions, but also for parton density (PDF) effects: at the LHC, the  $W$  and the  $Z$  are essentially sensitive to high- $Q^2$  sea partons, and a variation of these parameters will affect the  $W$  and  $Z$  distributions (in particular  $y^W, y^Z$ ) in a correlated way. Hence, the measurement of the  $Z$  distributions will help to control the  $W$  ones.

The simulation of QED radiation in  $W$  and  $Z$  decays was much improved recently [17, 25]. Still, the measurement of this process (through e.g.  $Z \rightarrow \ell\ell\gamma$ ) will allow to confirm the predictions. Other sources of uncertainty (e.g. backgrounds and underlying event) will also be controlled by auxiliary measurements at the LHC.

The following sections attempt to quantify the above arguments.

## 3 Experimental uncertainties

This section assesses the effect of efficiency and resolution in the reconstruction of leptons and missing transverse energy.

### 3.1 Lepton scale and resolution

The  $Z$  boson resonance has been measured very precisely at the lepton colliders during the 90's [3]. The  $Z$  boson mass and width can be exploited as an absolute reference to determine as precisely as possible the detector energy scale, its linearity and resolution.

The basic method is rather simple, and consists in comparing the position and width of the observed mass peak in reconstructed dilepton events with the  $Z$  boson parameters. A shift of the observed position of the mass peak, with respect to the nominal  $Z$  peak position, is corrected for by scaling the



detector response, hence determining the detector absolute scale; the additional spread of the mass distribution, as compared to the natural  $Z$  boson width, is used to estimate the resolution.

The high statistics expected at the LHC, however, imposes a number of refinements. First, the scale obtained as above is averaged over the lepton kinematical spectrum, whereas an energy-dependent scale is needed for a correct description of the Jacobian distributions in  $W$  events. Secondly, lepton energy resolution effects induce a small but non-negligible shift in the di-lepton invariant mass distribution. This shift needs to be subtracted before converting the scale measured from the  $Z$  invariant mass distribution into the scale used to describe the Jacobian distributions in  $W$  events. The resulting method has been described in detail in Ref. [26], and is summarized below.

### 3.1.1 Average detector scale

We first illustrate the energy-independent method, providing an average detector scale. Using the PYTHIA event generator [16], we produce a set of template histograms corresponding to generator-level  $Z$  lineshapes. The decay leptons are smeared and decalibrated with different energy scale factors  $\alpha$  and resolution functions  $\sigma$ . For definiteness, we consider calorimeter-like resolution functions parametrized as  $\sigma(E) = a \times \sqrt{E}$ . At this stage,  $\alpha$  is independent of the lepton energy. These templates are to be compared to the data; for our tests, we use an independently simulated sample as pseudo-data.

A  $\chi^2$  test is then performed between the pseudo-data and each of the template histograms, as in Section 2.2. This results in a two-dimensional  $\chi^2$  grid as a function of the smearing parameters. At the vicinity of the minimum, a paraboloid can be fitted through the points, and the parameters of this paraboloid give the estimates of the true values of  $\alpha$  and  $a$ .

The method is tested on a fully simulated  $Z \rightarrow ee$  sample, corresponding to 30700 events with  $85 < m_{ee} < 97$  GeV; the mass resolution can be treated as Gaussian over this range. We find an average resolution parameter  $a = 0.142 \pm 0.003$ , and an average mass scale  $\alpha = 1.0038 \pm 0.0002$ . Figure 3 illustrates the result, where the fully simulated  $Z \rightarrow ee$  lineshape is compared to an example template histogram assuming  $\alpha = 1$  and  $a = 0.12$ , and to the best fit result. Very good agreement is obtained; moreover, the ‘‘measured’’ scale and resolution parameters coincide with the values found when comparing the reconstructed electron energies to their generation-level values; the electron calibration in the fully simulated sample underestimates the true energy by 0.4%.

Assuming an inclusive  $Z$  production cross-section of 2 nb per leptonic decay channel and an integrated luminosity of  $10 \text{ fb}^{-1}$ , the average scale and resolution parameters can be controlled with a relative precision of  $\delta_{rel}\alpha = 2 \times 10^{-5}$  and  $\delta_{rel}a = 2 \times 10^{-4}$ . Note that these values are not far from the actual uncertainty of the  $Z$  boson parameters. As far as the absolute scale is concerned, a correlation between the induced  $W$ -mass systematic uncertainty and the  $Z$  boson mass uncertainty might finally appear.

As discussed in the introduction to this section, the method illustrated here has an important shortcoming: it only provides a scale averaged over the  $p_T^\ell$  distribution expected in  $Z$  events, which differs from that expected in  $W$  events. The averaged scale is applicable to  $W$  events only in the absence of any non-linearity in the detector response. In order to correctly propagate the  $Z$  calibration measurement to the  $W$  sample, the scale thus needs to be measured as a function of energy. This is discussed next.



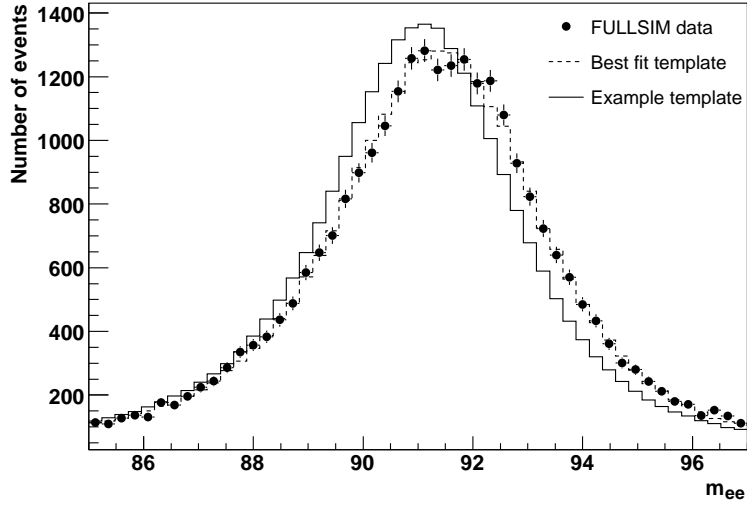


Figure 3: Comparison of a fully simulated  $Z \rightarrow ee$  sample (dots) to an initial template example, produced with  $\alpha = 1$  and  $a = 0.12$ , and to the best fit result.

### 3.1.2 Linearity: energy dependent scale and resolution

The above method can be extended as follows. The data and the templates are classified as a function of the lepton energies. This leads to templates and pseudo-data labeled  $(i, j)$ , corresponding to the event categories where one lepton falls in bin  $i$ , and the other in bin  $j$ . The scale factor  $\alpha_{ij}$  and the resolution parameter  $a_{ij}$  are then fitted in every bin.

In case of small non-linearities of the calorimetry response (i.e.  $\alpha_{ij}, \alpha_i, \alpha_j$  very close to 1), we can then derive the  $\alpha_i$  from the  $\alpha_{ij}$ , writing in first order approximation that the mass peak decalibration results from the decay lepton decalibrations:

$$\alpha_{ij} m_{12} = \sqrt{2 \alpha_i E_1 \alpha_j E_2 (1 - \cos \theta_{1,2})}, \quad \text{or} \quad (4)$$

$$\alpha_{ij} \sim (\alpha_i + \alpha_j)/2 \quad (5)$$

Writing this for every  $(i, j)$  gives a linear system which can be solved using least squares.

As for the resolution, the following linear system holds, neglecting the small contribution from the angular terms in the expression of the invariant mass resolution:

$$\frac{(\delta m_{ij}^2)^2}{m_{ij}^4} = \frac{\sigma_i^2}{E_i^2} + \frac{\sigma_j^2}{E_j^2} \quad (6)$$

which can again be solved using least squares, yielding the  $\sigma_i$ . We thus obtain the energy-dependent resolution function, independently of the form used to produce the templates.

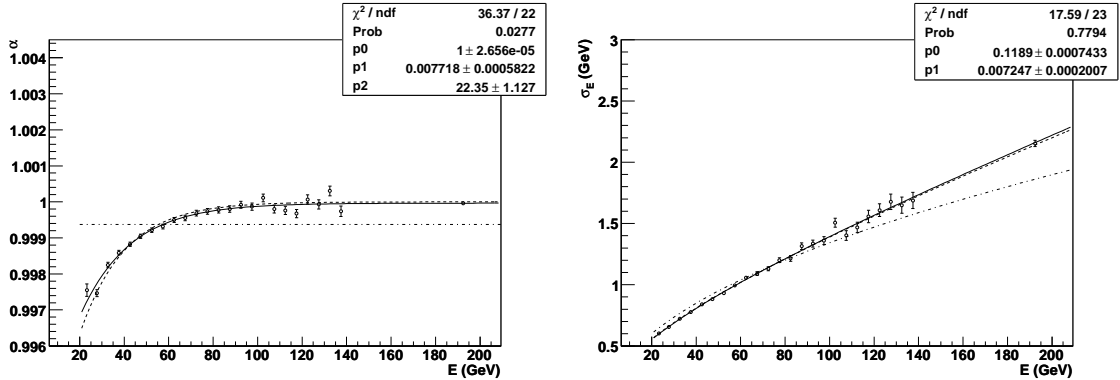


Figure 4: Left: reconstructed absolute energy scale, as a function of energy (points with error bars). The full line gives the injected function, representing the effect of non simulated passive material in front of the calorimeter. The dashed line is an empirical function fitted through the points; the dot-dashed line shows the result of an energy-independent analysis, missing the non-linearities. Right: reconstructed energy resolution (points with error bars). The full line is the true resolution function, of the form  $\sigma(E)/E = a/\sqrt{E} + b$ ; the dashed line is the reconstructed function. The dot-dashed line, assuming no constant term ( $b = 0$ ), is strongly excluded.

Examples of results that can be achieved are shown on Figure 4. With energy bins defined as intervals of 5 GeV, and a integrated luminosity of  $10 \text{ fb}^{-1}$ , the scale parameters are reconstructed with a precision of  $2 \times 10^{-4}$ , as estimated from the RMS of the  $\alpha$  residuals with respect to the injected function. Similarly, the resolution parameters are reconstructed with a precision of  $2 \times 10^{-3}$ .

### 3.1.3 Propagation to $m_W$ : $\delta m_W(\alpha_\ell)$ , $\delta m_W(\sigma_\ell)$

Assuming that bin-to-bin variations of the scale do occur with a spread of  $2 \times 10^{-4}$ , we can compute the impact of such variations on the measurement of  $m_W$ .

As described in Section 2, we perform a set of toy measurements, using the electron transverse momentum as observable, templates with varying  $m_W$  values but with a perfectly linear scale, and pseudo-data with fixed  $m_W$ , but containing non-linearities.

First of all, we can study the  $m_W$  bias as a function of the error on the average absolute scale. Not surprisingly, we find a strong dependence:

$$\frac{\partial m_W}{\partial_{\text{rel}} \alpha_\ell} \sim 800 \text{ MeV}/\%,$$

as illustrated in Figure 5.

In the case of an energy-dependent scale, the uncertainty on  $m_W$  is obtained by injecting random, energy-dependent decalibrations in the pseudo-data, with a spread corresponding to the result of the analysis of Section 3.1.2. With 480 independent exercises of this type, we obtain a distribution of  $m_W^{\text{fit}}$  as shown on Figure 6. The scale-induced  $W$  mass uncertainty is given by the spread of this distribution, and is  $\delta m_W(\alpha_\ell) = 4 \text{ MeV}$ .

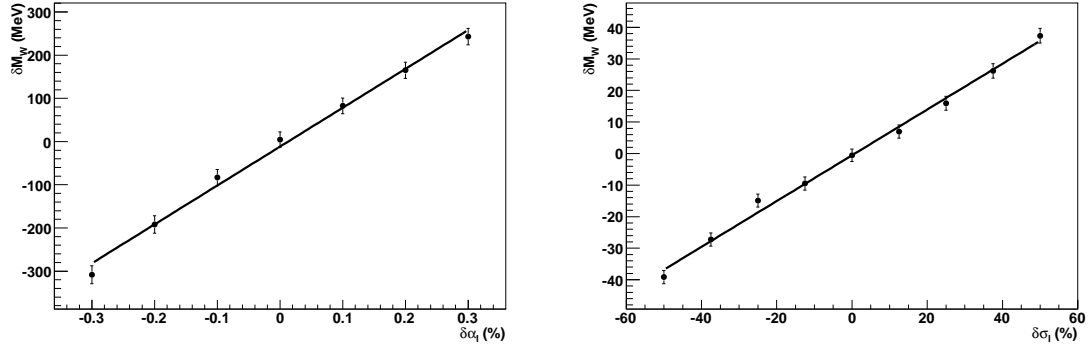


Figure 5: Left: bias on  $m_W$ ,  $m_W^{fit} - m_W^{true}$ , as a function of the relative bias on  $\alpha_\ell$ ,  $\delta\alpha_\ell = (\alpha_\ell^{fit} - \alpha_\ell^{true})/\alpha_\ell^{true}$ . Right: bias on  $m_W$  as function of the resolution bias,  $\delta\sigma_\ell = (\sigma_\ell^{fit} - \sigma_\ell^{true})/\sigma_\ell^{true}$ . A linear dependence is observed in each case, with  $\partial m_W/\partial_{rel}\alpha_\ell = 800$  MeV/% and  $\partial m_W/\partial_{rel}\sigma_\ell = 0.8$  MeV/%.

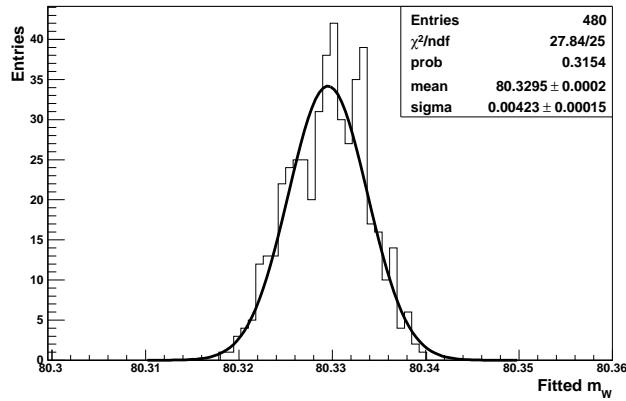


Figure 6: Distribution of  $m_W^{fit}$ , for 480 exercises with energy-dependent scale parameters randomly drawn within their uncertainties. The true mass is  $m_W = 80.33$  GeV; the systematic uncertainty is  $\sim 4$  MeV.

The effect of the resolution is studied by varying the resolution parameter in the pseudo-data, fitting to templates with fixed resolution, and collecting the corresponding values of  $m_W^{fit}$ . This provides the relation between the resolution bias and the resulting bias on  $m_W$ :

$$\frac{\partial m_W}{\partial_{rel} \sigma_\ell} = 0.8 \text{ MeV}/\%$$

as illustrated in Figure 5. Injecting the expected precision on the resolution, using the same method as above, yields  $\delta m_W(\sigma_\ell) \sim 1 \text{ MeV}$ .

The analysis presented here was originally done in terms of  $E$  (rather than transverse energy,  $E_T$ ) to ease comparison with the scale and linearity measurements performed on ATLAS testbeam data [27]. In the context of collision data, the analysis can instead be performed in terms of  $E_T$ ; the energy-dependent scale is reconstructed with the same precision as above, in the range  $20 < E_T < 70 \text{ GeV}$ . The propagation to  $\delta m_W(\alpha_\ell)$  and  $\delta m_W(\sigma_\ell)$  is unchanged.

In addition to the transverse energy dependence, the detector response is in general also a function of the lepton pseudorapidity  $\eta_\ell$ , azimuth  $\phi_\ell$ , and time. The physical  $\phi_\ell$  distributions are however uniform in general, and certainly for  $W$  and  $Z$  events. Hence it is safe to average over  $\phi_\ell$ ; any azimuthal dependence of the detector scale or resolution then acts as a contribution to the averaged detector resolution. Any possible time dependence of the energy response can be treated in the same way, provided the analysed  $W$  and  $Z$  event samples are taken from identical data taking periods (“runs”). It is however beneficial to limit the impact of this time dependence on the detector resolution by precisely monitoring its response as a function of time.

Although not strictly identical, the  $\eta_\ell$  distributions in  $W$  and  $Z$  events are also expected to be very similar within the detector acceptance (the difference is below 5% within  $|\eta_\ell| < 2.5$ , cf. Figure 7). As a first approximation, the same procedure can be applied; the averaging over  $\eta$  then assumes that leptons from  $W$  and  $Z$  are reconstructed with similar performance, with the same averaging contribution to the global detector resolution. The averaging can be improved by reweighting the  $\eta_\ell$  distribution observed in  $Z$  events, where the scale is measured, to reproduce the distribution observed in  $W$  events where the scale is applied. The detector response to leptons of given transverse momentum is then identical by construction in  $W$  and  $Z$  decays, up to the statistical precision of the reweighting. As will be seen in Section 6, the absolute scale determination is very stable against variations of the underlying physics hypotheses. In particular, it is negligibly affected by PDF uncertainties, which are the main factor determining the physical rapidity distribution of the  $Z$  boson and its decay products. The reweighting does thus not introduce hidden physics uncertainties, and does not affect the discussion of other systematic uncertainties.

The above analysis is performed on the example of the electron channels. As discussed in Section 2.2, the muon channels provide similar statistics, and are reconstructed with similar resolution. The present results thus equally hold in the electron and muon channels.

We end this section by noting that other well-known physics probes of detector scale exist, such as the low-mass vector resonances  $J/\Psi$  and  $\Upsilon$ . An over-constrained scale measurement can also be performed by first measuring the ID scale, exploiting muon final states; transporting the ID scale to the EMC, using the  $E/p$  distribution with isolated electrons; and finally verifying that this indirect EMC scale allows to reconstruct unbiased mass peaks for the known resonances in electron final states.

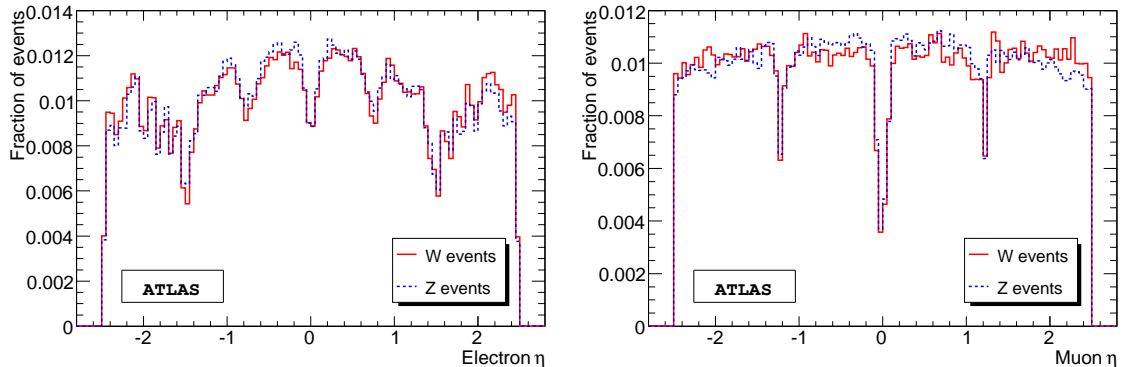


Figure 7: Electron (left) and muon (right)  $\eta$  distributions at reconstruction level, for  $W$  and  $Z$  events.

This confrontation of measurements is expected to allow to understand the source of any observed non-linearities in terms of magnetic field effects, imperfect alignment, excess of passive material in the detector, etc. It will thus be possible to confront several independent probes of the detector scale; compatibility between these measurements then validates its use for the measurement of  $m_W$ . This discussion is familiar from the Tevatron  $m_W$  measurements [9, 10]. The present analysis, using  $Z$  events only, quantifies the precision achievable at the LHC provided all measurements of the scale agree.

### 3.2 Lepton reconstruction efficiency

The observed Jacobian distributions in  $W$  events also reflect any  $p_T$  dependence of the lepton reconstruction efficiency. Any difference between the simulation used to produce the templates and the data will induce a distortion of the spectrum and cause a bias in the mass fit.

We again take the electron channel as our main example. The ATLAS electron identification largely exploits the shapes of their calorimetric showers [15], which have significant energy dependence. Hence, any selection based on these will have a  $p_T$ -dependent efficiency which has to be appropriately simulated in the templates. Unlike the electrons, no strong  $p_T$  dependence affects the muon reconstruction efficiency.

#### 3.2.1 Electron efficiency measurements

Electron reconstruction efficiency can be determined from the data with  $Z$  events, using e.g. the so-called “tag and probe” method [23], which we briefly summarize here.

Events are selected with one well-identified electron, and an additional high- $p_T$ , isolated track. The invariant mass of these two objects is required to be within 10 GeV from the nominal  $Z$  boson mass. Assuming that this selects  $Z$  events with enough purity, the identification efficiency is then obtained by computing the fraction of events where the second object is indeed identified as an electron. The efficiency of the isolation criterion is obtained in a similar way. Simulation studies show that the impact of backgrounds on the estimation of the efficiency is small compared to the statistical uncertainty.

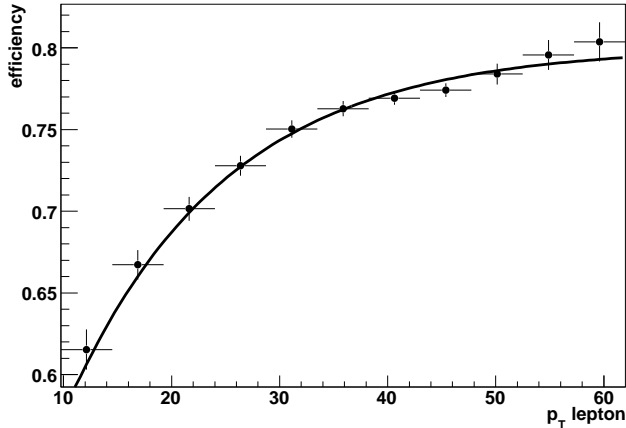


Figure 8: Electron reconstruction efficiency, as determined from fully simulated  $Z \rightarrow ee$  events.

For the present study we use about 200000 fully simulated  $Z \rightarrow ee$  events, from which the efficiency is evaluated. The result is shown in Figure 8, together with an empirical function describing main features of the  $p_T^e$  dependence. The following form:

$$\varepsilon(p_T) = \varepsilon_0 - a \exp(-b \times p_T) \quad (7)$$

correctly describes the efficiency in the  $p_T^e$  range relevant for the analysis.

### 3.2.2 Propagation to $m_W$ : $\delta m_W(\varepsilon)$

The effect of the efficiency uncertainty is estimated as in the previous section. Template distributions are produced at generator level, with varying values of  $m_W$ , and applying an efficiency factor according to the best fit efficiency function obtained above.

One hundred independent pseudo-data samples are generated at a fixed mass ( $m_W = 80.33$  MeV). Efficiency functions are applied with parameters drawn randomly within their uncertainties, as obtained in the previous section.

For each sample of pseudo-data, a fit is performed to the  $W$  mass. The fitted mass values are histogrammed, and the spread of the histogram gives the corresponding systematic uncertainty. With the efficiency determined using  $2 \times 10^5$   $Z$  boson decays, the efficiency-induced systematic  $W$  mass uncertainty is found to be  $\delta m_W = 33$  MeV. Other functional forms than Eq. 7 yield the same result. The most sensitive parameter in Equation 7 is  $b$ , the slope in the exponential. It is determined to be  $b = 0.068 \pm 0.006$ , corresponding to a precision of 9%; in other words,  $\partial m_W / \partial_{rel} b \sim 4$  MeV/%.

To emphasize the importance of this effect, the same pseudo-data samples are compared to templates assuming no  $p_T$ -dependence in the lepton reconstruction efficiency (i.e.  $f(p_T) = \text{constant}$ ). While the same spread is observed, the  $m_W^{fit}$  distribution indicates an average bias of about 450 MeV. This bias vanishes, to first order, when using the  $p_T$ -dependent efficiency in the templates.

$p_T$ cut	$\langle m_W^{fit} \rangle$ ( $\epsilon_{ref} = 1$ )	$\langle \delta m_W^{fit} \rangle$ ( $\epsilon_{ref} = 1$ )	$\langle m_W^{fit} \rangle$ ( $\epsilon_{ref} = f(p_T)$ )	$\langle \delta m_W^{fit} \rangle$ ( $\epsilon_{ref} = f(p_T)$ )
$p_T > 20$ GeV	80.78	0.033	80.34	0.033
$p_T > 34$ GeV	80.51	0.019	80.34	0.018
$p_T > 37$ GeV	80.44	0.013	80.33	0.012

Table 2: Average value of  $m_W^{fit}$  and its spread  $\delta m_W^{fit}$ , for several lower cuts on the  $p_T$  range used in the mass fit. Numbers are given as obtained from templates assuming a flat efficiency (second and third column), and using the efficiency measured in  $Z$  events (fourth and fifth column).  $m_W^{true} = 80.33$  GeV.

Extrapolating to  $10 \text{ fb}^{-1}$ , i.e. assuming  $3 \times 10^6$  measured  $Z$  boson decays, an improvement of a factor  $\sim 4$  is expected in the efficiency determination. Correspondingly, we obtain  $\delta m_W(\epsilon) \sim 8$  MeV.

### 3.2.3 Discussion and improvements

As can be seen in Figure 8, the electron efficiency varies most rapidly when  $p_T^e \sim 20$  GeV, and is much flatter around the Jacobian edge. Until now, the full  $p_T^e$  spectrum, selected as described in Section 2, has been used in the mass fits.

The effect of restricting the lepton  $p_T^e$  range used in the fit to higher values is displayed in Table 2. Considering the part of the spectrum verifying  $p_T^e > 34$  GeV, for example, reduces  $\delta m_W$  from 33 MeV to 18 MeV. While avoiding the region with strongest  $p_T$ -dependence of the efficiency, the Jacobian edge is still fully exploited, and the statistical sensitivity is almost unaffected. Extrapolating to  $10 \text{ fb}^{-1}$ , we obtain a remaining uncertainty of  $\delta m_W(\epsilon) \sim 4.5$  MeV.

Note that the results presented here reflect the state of the ATLAS reconstruction software at the time of writing this paper. Significantly improved algorithms are described in Ref. [21], notably resulting in a smaller  $p_T$ -dependence of the electron reconstruction efficiency. The related systematic uncertainty on  $m_W$  should decrease accordingly. The numbers presented here may thus be considered as conservative.

For muons with sufficient momentum to cross the whole detector ( $p > 6$  GeV), no source of inefficiency has a strong  $p_T$  dependence. Hence, the corresponding induced uncertainty on  $m_W$  is smaller. The above estimate is thus conservative when applied to the muon channel.

## 3.3 Recoil scale and resolution

When using the  $m_T^W$  distribution in the mass fit,  $p_T^V$  enters the definition of the observable. This quantity, measured experimentally as the vector sum of the transverse energy of all reconstructed detector signals (high- $p_T$  leptons and low- $p_T$  hadronic activity), needs to be precisely described by the simulation for the same reasons as above.

### 3.3.1 Sensitivity to the recoil scale with $Z$ events

The  $W$  and  $Z$  bosons are produced through very similar partonic processes, and thus one expects the spectator part of the event (the underlying event) to behave similarly, up to the small phase space



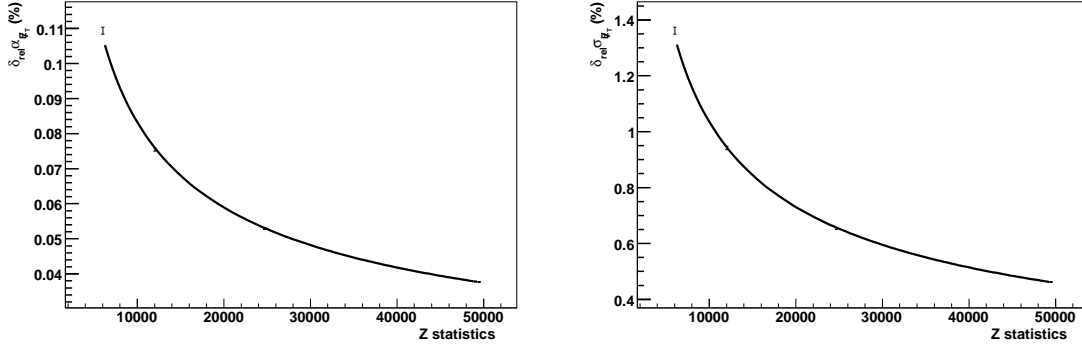


Figure 9: Left: statistical sensitivity to  $\alpha_{E_T^{miss}}$ , as a function of the accumulated Z statistics. Right: statistical sensitivity to  $\sigma_{E_T^{miss}}$ .

difference ( $m_W \neq m_Z$ ).

Assuming that the absolute lepton scale and resolution have been measured beforehand (cf. Section 3.1), one can measure the recoil scale ( $\alpha_{rec}$ ) and resolution ( $\sigma_{rec}$ ) in fully reconstructed Z events, where no significant  $E_T^{miss}$  is expected, by comparing the measured hadronic energy  $E_{rec}$ , recoiling against the Z boson, to the reconstructed di-lepton four-momentum,  $p_T^{\ell\ell}$ . Specifically,  $\alpha_{rec}$  and  $\sigma_{rec}$  are extracted from the peak position and spread of the distribution of  $E_{rec}/p_T^{\ell\ell}$ . The results can then be used to correct the observed recoil, and hence  $E_T^{miss}$ , in W events.

Figure 9 shows the expected sensitivity to  $\alpha_{rec}$  and  $\sigma_{rec}$ . With  $10 \text{ fb}^{-1}$ , these parameters can be determined with a statistical precision of  $\delta\alpha_{rec} = 5 \times 10^{-5}$  and  $\delta\sigma_{rec} = 6 \times 10^{-4}$ .

### 3.3.2 Propagation to $m_W$ : $\delta m_W(\alpha_{E_T^{miss}})$ , $\delta m_W(\sigma_{E_T^{miss}})$

The effect on  $m_W$  is evaluated by systematically varying the recoil scale, producing corresponding pseudo-data samples as in the previous sections, and fitting each sample to perfectly calibrated templates. We obtain the relation between the  $m_W$  bias and the recoil scale and resolution in the form of a derivative:

$$\frac{\partial m_W}{\partial_{rel} \alpha_{E_T^{miss}}} = -200 \text{ MeV}/\% \quad \frac{\partial m_W}{\partial_{rel} \sigma_{E_T^{miss}}} = -25 \text{ MeV}/\%$$

as illustrated in Figure 10. Injecting  $\delta\alpha_{E_T^{miss}} = 5 \times 10^{-5}$ , we obtain a systematic uncertainty of  $\delta m_W(\alpha_{E_T^{miss}}) = 1 \text{ MeV}$ . Similarly, we find the contribution from the resolution to be  $\delta m_W(\sigma_{E_T^{miss}}) = 1.5 \text{ MeV}$ . These numbers assume that the Z-based calibration can be transported to the W sample without additional uncertainty; this is discussed further below.

### 3.3.3 Further discussion

The  $E_T^{miss}$  calibration can be studied in more detail, using real Z events where one reconstructed lepton is artificially removed. In the case of electrons, the removed calorimetric energy should be properly

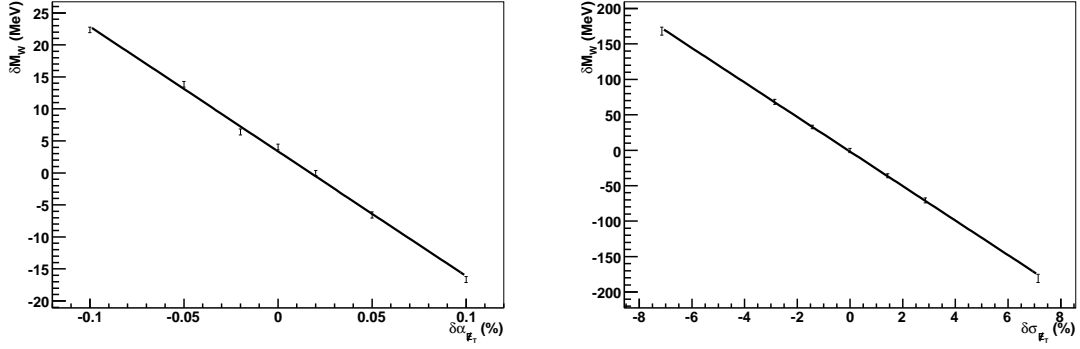


Figure 10: Left: Bias on  $m_W$ ,  $\delta m_W = m_W^{fit} - m_W^{true}$ , as a function of the bias on the recoil scale,  $\delta \alpha_{E_T^{miss}}$ . Right:  $\delta m_W$  as function of the resolution bias,  $\delta \sigma_{E_T^{miss}}$ . A linear dependence is observed in each case, with  $\partial m_W / \partial_{rel} \alpha_{E_T^{miss}} = -200 \text{ MeV}/\%$  and  $\partial m_W / \partial_{rel} \sigma_{E_T^{miss}} = -25 \text{ MeV}/\%$ .

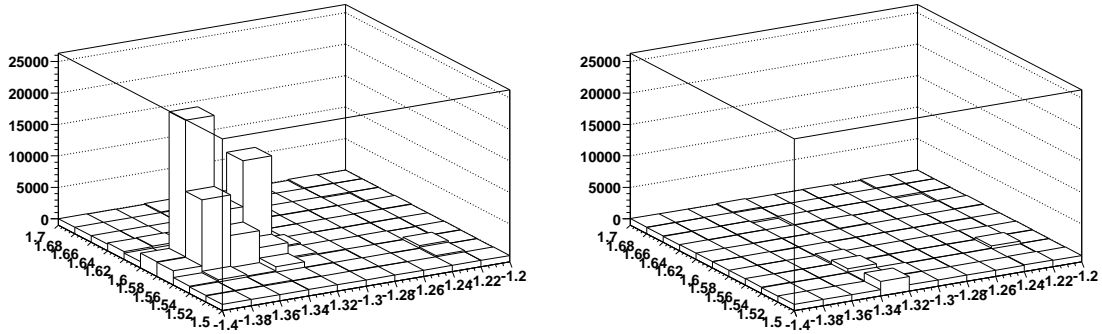


Figure 11: Left: electron cluster in a  $Z \rightarrow ee$  event. Right: the same calorimeter region, after the cluster has been removed. The energy in each cell belonging to the electron cluster is replaced by a number drawn from a Gaussian with mean and RMS corresponding to detector noise.

replaced by the expected noise. For muons, also, the minimum-ionizing energy depositions in the calorimeters need to be removed and replaced by the expected noise as above. The resulting events mimic  $W$  events and have a precisely known missing energy, corresponding to the energy of the removed lepton, which can be compared to the result of the  $E_T^{miss}$  reconstruction algorithm.

The lepton removal requires that one can identify and remove the electron signal from the struck calorimeter cells, while leaving a realistic contribution from noise and hadronic background (see Figure 11). Several approaches can be tried, such as replacing the contents of the electron cluster cells by energy measured away of any high- $p_T$  object in the event (e.g. at  $90^\circ$  in azimuth), or by the average expected electronic and hadronic noise.

To determine the  $E_T^{miss}$  resolution and possibly correct for biases in its measurement, we consider the reconstructed  $E_T^{miss}$  of  $Z \rightarrow \ell\ell$  events before and after the removal of one lepton, and compare the

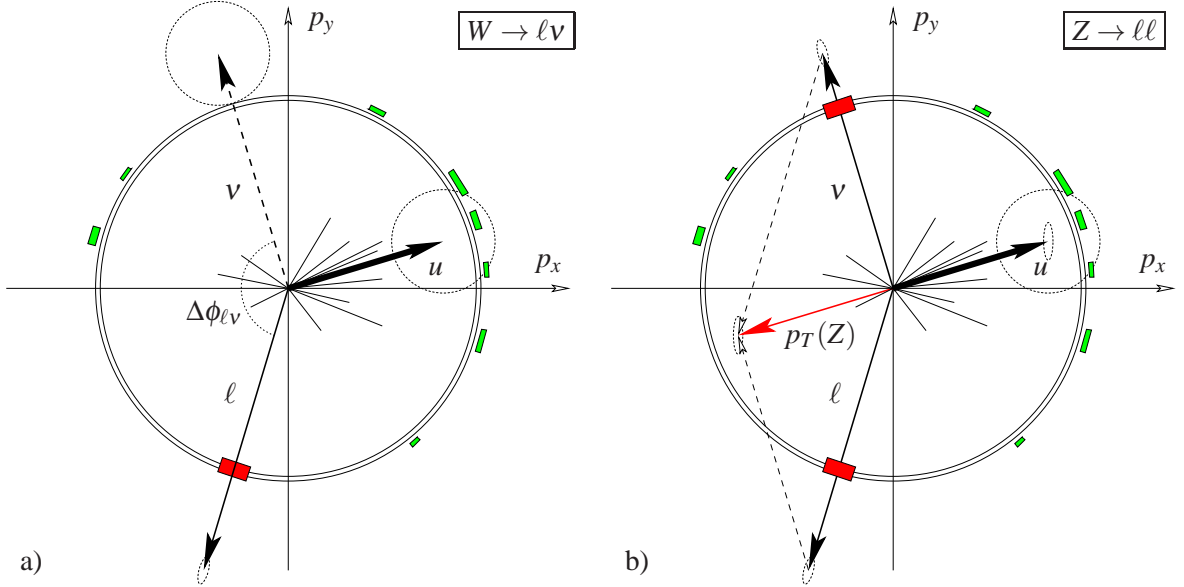


Figure 12: Transverse view of a)  $W \rightarrow \ell\nu$  and b)  $Z \rightarrow \ell\ell$  events. The combined transverse momentum of the recoil  $u$ , which should match that of the boson, is used to estimate the momentum of the undetected neutrino in the  $W \rightarrow \ell\nu$  decay. The  $Z$  boson line of flight is represented, which defines the  $(\parallel, \perp)$  coordinate system. The size of the dotted ellipses represent the resolution on the reconstructed objects.

difference to the transverse momentum of the removed lepton. A non-zero average value of this difference points to a bias in the  $E_T^{miss}$  reconstruction.

Rather than projecting this difference on conventional X and Y axes in the transverse plane, it is best to consider the natural frame of the event, with axes parallel ( $\parallel$ ) and perpendicular ( $\perp$ ) to the  $Z$  boson transverse momentum. Imperfect calibration of the  $E_T^{miss}$  reconstruction will show up as biases in these distributions, which can then subsequently be corrected for within statistics. The axes are illustrated in Figure 12.

This method is tried on a fully simulated sample of  $Z \rightarrow ee$  events, with results illustrated in Figure 13. As can be seen in this example, a bias is observed in the  $E_T^{miss}$  reconstruction along the  $Z$  line of flight. No bias is observed along the other axes. In this example, the calibration is thus correct on average, but the  $E_T^{miss}$  reconstruction does not respond perfectly to the event-by-event topology.

As this discussion illustrates,  $E_T^{miss}$  reconstruction is a very difficult experimental algorithm to control, especially to the level of precision desired here. Therefore, we cannot claim at present that the sensitivity quoted in the previous section will indeed be reached. Instead, lacking the proof that the statistical enhancement can be fully exploited, we assume an overall uncertainty of  $\delta m_W(E_T^{miss}) = 5$  MeV. This number is a factor 3 higher than the purely statistical sensitivity, and a factor three smaller than the systematic uncertainty obtained in the recent CDF measurement [10] based on an integrated luminosity of  $200 \text{ pb}^{-1}$  and about 8000  $Z$  events for calibration of the hadronic recoil.

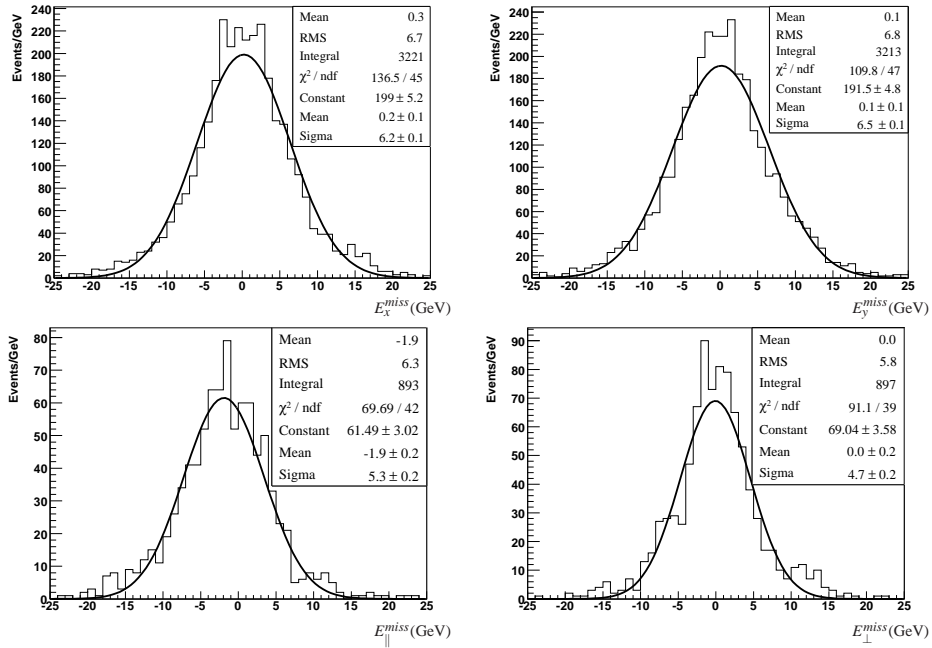


Figure 13: Top: resolution on  $E_T^{\text{miss}}$ , projected onto the (X, Y) coordinate system, for unmodified, fully simulated  $Z \rightarrow ee$  events. Bottom:  $E_T^{\text{miss}}$  resolution in the ( $\parallel$ ,  $\perp$ ) coordinate system. The absence of bias along the X and Y axes show that the overall calibration is correct on average, but the observed bias along the  $\parallel$ -axis, corresponding to the Z line of flight, indicates imperfect calibration of the response to the event-by-event topology.

## 4 Theoretical uncertainties

We discuss below the uncertainties related to imperfect physics modeling of  $W$  production. The correlation of the mass measurement with the  $W$  width, the impact of final state radiation, and biases in the  $p_T^\ell$  and  $m_T^W$  distributions induced by  $p_T^W$  and  $y^W$  distortions are discussed in turn.

### 4.1 $W$ boson width: $\delta m_W(\Gamma_W)$

A change in the  $W$  width  $\Gamma_W$  affects the Jacobian peak, and can cause a bias in the  $W$  mass measurement. To assert the size of this effect, samples with the same  $W$  mass but  $W$  widths varying in the range 1.7 – 2.5 GeV were produced and subsequently fitted. The relation between  $\Gamma_W$  and  $m_W$  in the fit is linear, with a slope depending on the distribution used in the mass fit. If the  $W$  transverse mass is used, we find:

$$\frac{\partial m_W}{\partial_{rel}\Gamma_W} = 3.2 \text{ MeV}/\%$$

If the lepton transverse momentum is used, we find:

$$\frac{\partial m_W}{\partial_{rel}\Gamma_W} = 1.2 \text{ MeV}/\%$$

The intrinsic width of the  $W$  resonance  $\Gamma_W$  has been measured to be  $2.141 \pm 0.041$  GeV, while the SM prediction is  $2.0910 \pm 0.0015$  GeV [28]. It should be taken into account that the LHC data can be expected to improve the precision on the  $W$  width as well as on  $m_W$ . Earlier measurements of  $\Gamma_W$  [29, 30] are affected by the same systematic uncertainties as those discussed in this paper. Hence, anticipating on our results, we assume that an improvement by a factor five should be achievable, respectively leaving  $\delta m_W(\Gamma_W) = 1.3$  and 0.5 MeV for the  $m_T^W$  and  $p_T^\ell$  fits.

### 4.2 QED final state radiation: $\delta m_W(QED)$

Final state radiation causes significant distortions of the naive, lowest order  $p_T$  spectrum of the  $W$  decay leptons. We estimate the stability of the theoretical calculation below, using the PHOTOS program [17] as a benchmark.

The numerical importance of final state radiation is illustrated in Figure 14, which displays the distribution of the measured lepton energy fraction (relative to their energy in the absence of FSR). For electrons, measured *via* calorimetric energy clusters, most of the (collinearly radiated) photon energy is collected in the cluster. The momentum of muons tracks, on the contrary, is measured independently of any photon radiation. The average values of the distributions lie at about 99% of the original value, meaning that ignoring the effect entirely would cause a bias on the  $W$  mass of about 800 MeV. The theoretical stability of the calculation is thus of critical importance.

In recent versions of PHOTOS, it is possible to switch between several theoretical assumptions. In particular,  $W$  and  $Z$  boson decays can be simulated with photon emission up to  $O(\alpha)$ ,  $O(\alpha^2)$ ,  $O(\alpha^4)$ , or with photon emission exponentiation [31]. To study the model differences, we have generated about  $10^6$  events for each setting, and for each production and decay channel ( $W \rightarrow \ell\nu$ ,  $Z \rightarrow \ell\ell$ , for  $\ell = e, \mu$ ).

The average values of the energy fractions discussed above are shown in Figure 15, for successive theoretical refinements. The different average values for electrons and muons reflect the different

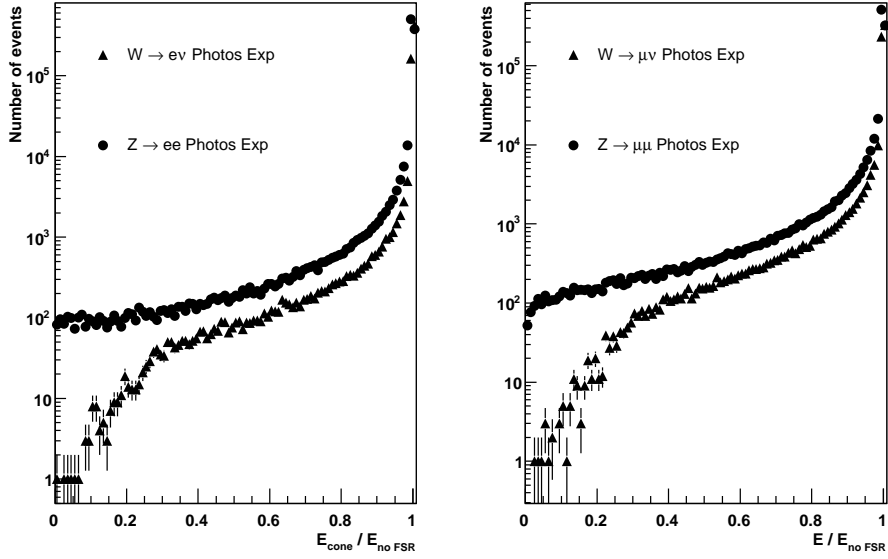


Figure 14: Distribution of the measured lepton energy fraction (i.e. relative to their energy in absence of FSR). PHOTOS is run in exponentiated mode. The energy of electrons is measured dressed with all photon energy radiated within a cone of radius 0.1, corresponding to the size of reconstructed EM clusters. Muon momentum is measured bare, after FSR.

ways their energy or momentum is measured. The calculation appears stable to about  $1-2 \times 10^{-4}$ , the residual differences being compatible with coming from the finite sample statistics only. It is unfortunately not practical to further increase the samples sizes and quantify the stability to better precision.

To improve on the above argument, consider the  $Z$  boson mass measurement at LEP1 [3]. Similarly to our case, QED corrections, in the form of initial state radiation off the electron beams, have a large impact on the  $Z$  lineshape, inducing a decrease of the cross-section of about 30%, and a shift of the peak position of about 100 MeV. Nevertheless, the theoretical uncertainty on these effects are estimated to 0.3 MeV, compared to a total measurement uncertainty of 2.1 MeV. The theory of QED radiation thus carries negligible uncertainty.

For the QED induced  $m_W$  uncertainty to be as small, the event generators used to produce our templates thus need to have similar theoretical accuracy, with the additional complication that the present analysis requires an exclusive description of the final state (i.e. a complete description of the photon distributions), whereas the  $Z$  lineshape analysis only relies on the effective energy of the beams after radiation. In Ref. [32], the accuracy of the PHOTOS algorithm is upgraded to NLO accuracy. Similarly, the HORACE event generator [25] contains QED and weak corrections to NLO accuracy. Both programs implement photon emission exponentiation.

We thus assume that ultimately  $\delta m_W(QED) \leq 1$  MeV can be reached. This assumption is conditioned by the availability of the necessary tools in time for the measurement.

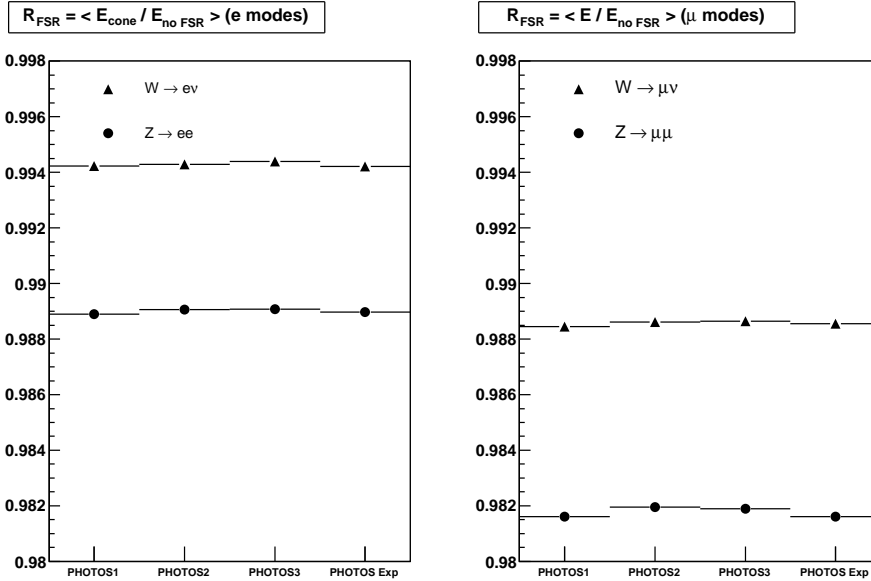


Figure 15: Averages of the distributions of Figure 14, for various PHOTOS settings (see text).

Let us finally note that  $W$  and  $Z$  events behave differently under QED radiation. The average energy fraction in  $Z$  events is  $5\text{-}7 \times 10^{-3}$  smaller than in  $W$  events, depending on the final state. The energy scale measurement (cf. Section 3.1) and the  $W$  mass measurement should properly account for the difference in the respective QED radiation patterns. We will come back to this point in Section 6.

### 4.3 $W$ distributions

The  $W$  rapidity and transverse momentum distributions result from the interplay of the proton structure functions, and strong interaction effects at the  $W$  production vertex. To simplify the discussion, we will consider the longitudinal and transverse distributions independently, as respective results of parton distributions and QCD higher orders.

#### 4.3.1 Rapidity distribution: $\delta m_W(y^W)$

The  $W$  rapidity distribution is essentially driven by the proton parton density functions (PDFs). Our study is based on the CTEQ6.1 structure functions sets [33], which provide, in addition to the global best fit, PDFs corresponding to the variation of each diagonal parameter (i.e., the linear combination of input parameters that diagonalize the covariance matrix) within its estimated uncertainty. The PDF-induced uncertainty for an observable is obtained by computing its value with all sets, taking the central value as given by the best fit, and quadratically summing the biases (w.r.t the best fit value) obtained from the uncertainty sets.

As illustrated in Figure 16 (see also Ref. [14]), the current PDF uncertainties induce an uncertainty in the  $W$  rapidity distributions which, through acceptance effects, propagates a systematic uncertainty on the  $W$  mass determination of  $\sim 25$  MeV. We present below an attempt to estimate how this will



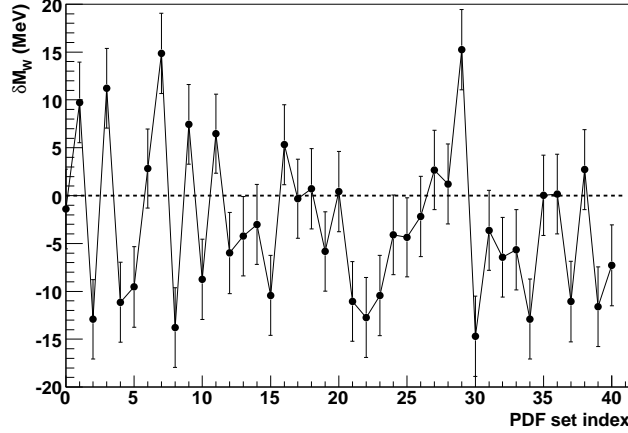


Figure 16: Bias on  $m_W$  obtained when varying the proton PDFs within their uncertainties. Each point on the abscissa corresponds to a given PDF set: set 0 is the best fit, and gives 0 bias up to the statistical uncertainty of the fit; sets 1-40 are the uncertainty sets, each inducing a given bias on  $m_W$ . The total uncertainty on  $m_W$  is given by the quadratic sum of the biases, giving  $\delta m_W \sim 25$  MeV.

improve with the LHC data.

At the LHC,  $W$  and  $Z$  particles are essentially produced through sea quark interactions; the influence of valence quarks is small. Low- $x$ , high- $Q^2$  sea quarks mainly evolve from higher  $x$ , lower  $Q^2$  gluons, and a consequence from perturbative QCD flavour symmetry is that up to initial asymmetries and heavy-quark mass effects, the different quark flavours should be represented democratically. This then implies that the impact of sea quark PDF uncertainties on  $W$  and  $Z$  production should be very similar. In other words, when varying PDFs within their uncertainties, one expects a strong correlation between the induced variations of the  $W$  and  $Z$  distributions.

This is confirmed by Figure 17 <sup>1)</sup>. On the left, the correlation between the widths of the  $W$  and  $Z$  boson rapidity distributions is displayed. We choose to use the distributions RMS, denoted  $r_y^W$  and  $r_y^Z$ , to quantify their width. The current CTEQ6.1 prediction,  $r_y^Z = 2.16 \pm 0.03$ , will be refined to a precision of  $\delta r_y^Z = 0.001$ . Exploiting Figure 17 (right), which quantifies the correlation between  $r_y^W$  and  $r_y^Z$ , this can be translated into a prediction of the  $W$  boson rapidity distribution,  $\delta r_y^W = 0.0013$ , to be compared to the current prediction  $r_y^W = 2.24 \pm 0.03$ .

One thus expects an improvement on the  $Z$  rapidity distribution by a factor  $\sim 30$ . This is also illustrated in Figure 18, where two extreme predictions (with current knowledge) of the  $Z$  rapidity distribution are compared with an example distribution representing the same measurement. Given the residual decorrelation between the  $W$  and  $Z$  distributions, this translates into an improvement on the  $W$  rapidity distribution by a factor  $\sim 23$ .

Starting with  $\delta m_W(y_W) \sim 25$  MeV, putting in a precise measurement of the  $Z$  rapidity distribution at

<sup>1)</sup>This plot is reminiscent of Figure 2 in [34], displaying similar correlations in the production rates. Note that for our purpose, normalizations are irrelevant and we are interested only in the distributions.

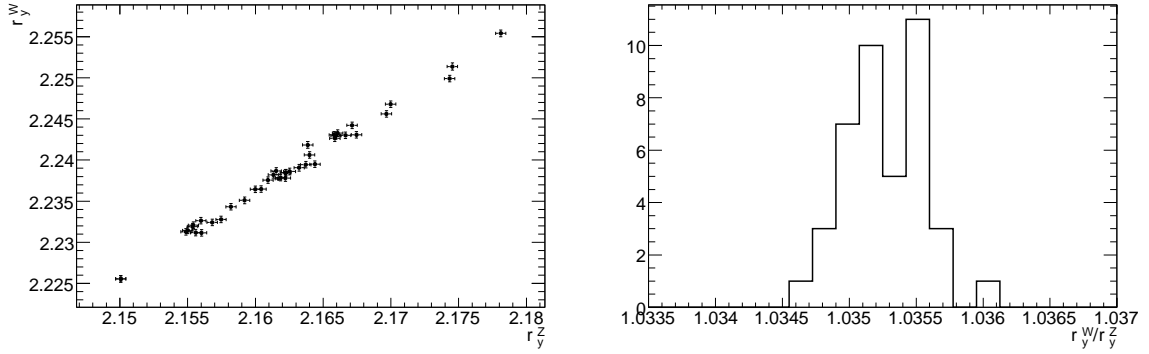


Figure 17: Left : correlation between the spreads (RMS)  $r_y^W$  and  $r_y^Z$  of the  $W$  and  $Z$  rapidity distributions, when varying the CTEQ6.1 PDFs within their estimated uncertainties. The fitted pseudo-data are scaled to an integrated luminosity of  $10 \text{ fb}^{-1}$ . Right : distribution of the ratio  $r_y^W / r_y^Z$ , again varying the PDFs within their uncertainties. The spread of the ratio distribution is  $4 \times 10^{-4}$ .

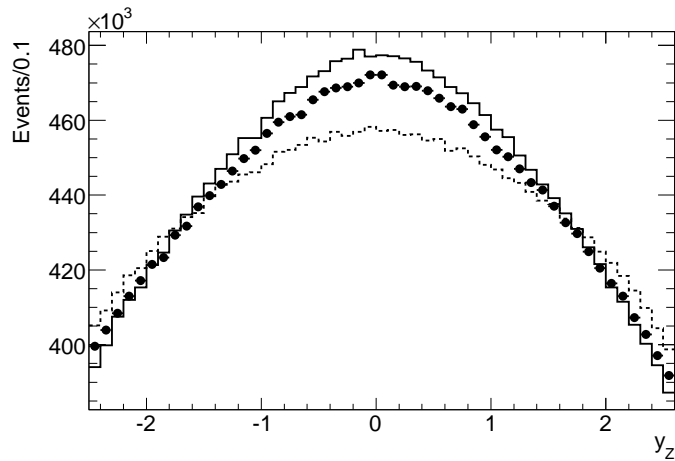


Figure 18: The line histograms represent two extreme predictions for the  $Z$  rapidity distribution, as given by the CTEQ6.1 PDF sets. The points are pseudo-data, obtained with the central set, and scaled to an integrated luminosity of  $10 \text{ fb}^{-1}$ .

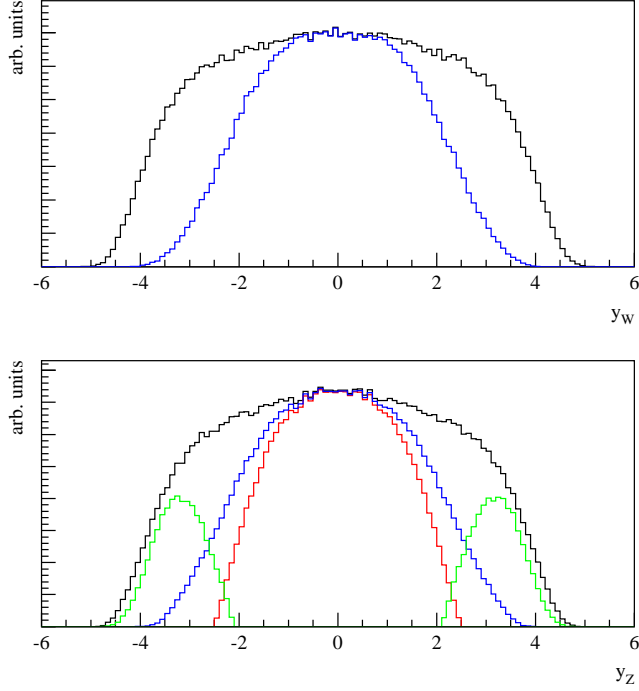


Figure 19: Upper plot: the outer histogram represents the complete rapidity distribution for  $W$  production at the LHC; the inner histogram represents the range selected by the condition  $|\eta_\ell| < 2.5$ . Lower plot: the outer histogram represents the complete rapidity distribution for  $Z$  events. The innermost histogram is obtained requiring two decay leptons within  $|\eta_\ell| < 2.5$ ; the intermediate histogram is obtained when allowing one electron within  $|\eta_\ell| < 4.9$ . The two symmetric histograms at high rapidity correspond to the LHCb muon acceptance.

the LHC, and exploiting the strong correlation between the  $W$  and  $Z$  production mechanisms, we thus anticipate a final uncertainty from the description of the  $W$  rapidity distribution of  $\delta m_W(y_W) \sim 1$  MeV.

In practice, the analysis will of course proceed *via* a formal QCD analysis to the LHC data: the measured  $Z$  differential cross-section  $d\sigma/dy$ , together with other measurements (see below), will be fed to parton distribution fits, and the systematic  $\delta m_W(y^W)$  from the improved PDF sets will be evaluated as above. The present discussion however allows to estimate the expected improvement while avoiding these complications.

Let us also note that  $Z$  rapidity distribution can be analyzed over a domain that fully includes the range relevant for  $W$  production. In ATLAS (as in CMS), the usual  $Z$  acceptance, given by  $|\eta_\ell| < 2.5$  for both decay leptons, can be extended in the electron channel by allowing one of the electrons to be detected within  $|\eta_e| < \sim 4.9$ . In addition, high-rapidity  $Z$  events will be produced and detected at LHCb (for example, the geometric acceptance of the muon detector is approximately  $2.1 < |\eta_\mu| < 4.8$ ). Accounting for this, and as illustrated in Figure 19, the  $W$  rapidity range selected for the  $m_W$  measurement is entirely included in the  $Z$  one. This remains true in terms of the parton momentum fractions.

We conclude this section with some caveats. The above results partly are a consequence of the as-

sumed flavour and charge symmetry in the low- $x$  proton; notably, the parton parametrisations used in the fits used above assume that  $d(x) = \bar{d}(x) = u(x) = \bar{u}(x)$  at low- $x$ , and  $s = \bar{s}$  at all  $x$ . This implies the strong correlation discussed above, since the  $Z$  production rate is proportional to  $u\bar{u} + d\bar{d} + \dots$ , and the  $W$  rate is proportional to  $u\bar{d} + d\bar{u} + \dots$ . It is thus important to quantify the dependence of our result on these hypotheses.

The anti-quark flavour asymmetry  $\bar{u} - \bar{d}$  was measured to be non-0 in the region  $0.015 < x < 0.35$ , and  $Q^2 \sim 50 \text{ GeV}^2$  [35, 36], in contradiction with the flavour symmetry assumption. The relative asymmetry,  $(\bar{u} - \bar{d})/(\bar{u} + \bar{d})$ , is however of the order  $\sim 10^{-2}$ , decreasing towards higher  $Q^2$ . Starting from  $\bar{u} = \bar{d}$  and full correlation between  $W$  and  $Z$  production (i.e.  $W$  and  $Z$  distributions have the same rate of change under PDF variations),  $\bar{u} \neq \bar{d}$  induces a decorrelation of order  $(\bar{u} - \bar{d})/(\bar{u} + \bar{d}) \times (u - d)/(u + d)$ , where both factors are of order  $10^{-2}$  (see for example Figure 1 in [33]). Hence, even in the presence of non-vanishing  $\bar{u} - \bar{d}$ , the freedom of the  $W$  distributions is very limited once  $Z$  ones have been precisely measured. We thus assume that our estimates remain correct; nevertheless, measurements of the  $W$  charge asymmetry, sensitive to  $\bar{u} - \bar{d}$ , will allow to verify this hypothesis. Additional information will be provided by measuring  $m_W$  in  $W^+$  and  $W^-$  events separately.

The proton strangeness asymmetry,  $s(x) - \bar{s}(x)$ , is constrained by neutrino scattering data [37–39]. The relative asymmetry is rather small, even at low  $Q^2$ :  $(s - \bar{s})/(s + \bar{s}) \sim 10^{-2}$  at  $Q^2 = 10 \text{ GeV}^2$ . It will only become smaller at  $Q^2 \sim m_W^2$ , where most of the strange sea is generated radiatively. We consider, as above, that the contribution of the asymmetry is small in terms of the overall  $W$  production and its uncertainty. However, the impact on the  $m_W$  measurement would need to be studied specifically. At the LHC, the analysis of  $W^{-/+} + c/\bar{c}$  production should provide additional insight.

Finally, one may argue that the influence of heavy quark PDFs on  $W$  and  $Z$  production is different, thus a source of decorrelation between the two processes. The charm quark contribution to  $W$  production is significant ( $\sim (V_{cs}c\bar{s} + V_{cd}c\bar{d} + c.c.)$ ), but smaller for  $Z$  production ( $\sim c\bar{c}$ ). On the other hand, the  $b$ -quark content contributes to  $Z$  production ( $\sim b\bar{b}$ ), but negligibly to  $W$  production ( $\sim (V_{cb}c\bar{b} + c.c.)$ ), due to the smallness of the off-diagonal third generation CKM matrix elements. These differences are however accounted for by the present analysis, since the heavy quark PDFs are included the CTEQ6.1 PDF sets; heavy flavours are actually understood to cause in part the small decorrelation between the  $W$  and  $Z$  boson distributions. Our conclusions thus remain unchanged.

The present study has been repeated using the MRST2001 PDF sets [40]. The same correlation is observed between  $r_y^W$  and  $r_y^Z$ , and the same result is obtained. Non-global parton density fits, such as those performed by the H1 and Zeus experiments, are based on similar hypotheses and claim slightly smaller uncertainties [41], again preserving our result. Finally, during the course of this work, CTEQ6.5 PDF sets became available [42], which improves on the treatment of heavy quark masses in the QCD evolution. The flavour symmetry assumptions are however unchanged, so that the present discussion is not affected.

### 4.3.2 Transverse momentum distribution: $\delta m_W(p_T^W)$

The prediction of vector boson  $p_T$  distributions at hadron colliders has long been an active subject [24, 43, 44]. It is also a crucial input for the  $W$  mass analysis, especially when using the  $p_T^\ell$  observable. We discuss below the impact of  $p_T^W$  uncertainties on the  $W$  mass determination in this hypothesis.

The measurable  $p_T^W$  and  $p_T^Z$  distributions are the result of several effects, most notably the repeated, partly non-perturbative parton radiation occurring in the transition from the low- $Q^2$  proton towards the hard process (commonly referred to as parton showers, or soft gluon resummation). Another source is the transverse momentum intrinsic to the partons in the proton. We choose not to discuss these effects separately. Rather, reckoning that although  $W$  and  $Z$  production differ in several respects (the coupling to initial partons is different in both phase space and flavour), the non-perturbative mechanisms are universal, we evaluate how precisely their combined effect can be measured in neutral current events, and how this improves the  $W$  predictions. Notice that heavy flavour PDF have caused only a small decorrelation between  $W$  and  $Z$  events in the previous section; this is assumed to remain true in this discussion.

First, the relation between the bias in the modeling of  $p_T^W$  and the measurement of  $m_W$  is investigated by applying scaling factors to the  $p_T^W$  distributions in our pseudo-data, deducing the corresponding  $p_T^\ell$  distributions, and fitting  $m_W$  against un-distorted templates. The bias in  $m_W$  appears to be a linear function of the  $p_T^W$  mis-modelling, with a slope of order 0.3, meaning a 3 MeV bias on  $p_T^W$  results in a 1 MeV bias on  $m_W$ , when exploiting the  $p_T^\ell$  distribution. When  $m_T^W$  is used, the effect is negligible.

Neutral current dilepton events allow to measure the  $p_T^{\ell\ell}$  distribution, as a function of mass, over a large mass range. Assuming usual selections, this distribution will be measured precisely for  $30 < M_{\ell\ell} < \sim 200$  GeV. This large lever arm, in addition to the very precise determination of the  $p_T^{\ell\ell}$  distribution on the  $Z$  peak, provides a precise control of  $d\sigma/dp_T^{\ell\ell}$  when  $M_{\ell\ell} \sim m_W$ . This is illustrated in Figure 20, which displays the dilepton mass dependence of its average transverse momentum,  $\langle p_T^{\ell\ell} \rangle$ , as predicted by PYTHIA.

On the  $Z$  peak,  $p_T^{\ell\ell}$  will be known to about 7 MeV with an integrated luminosity of  $10 \text{ fb}^{-1}$ . Thanks to the Drell-Yan continuum, the accuracy in the region of  $m_W$  is still  $\sim 8$  MeV. This precision can be used to constrain the non-perturbative parameters governing the parton shower or resummation computations, and to predict the  $p_T^W$  distribution with similar accuracy. This leads to an uncertainty on  $m_W$  of about 3 MeV.

Arguably, the  $p_T^W$  distribution cannot be summarized by its mean value. However, in the low  $p_T^W$  region (selected by the recoil cut, cf. Section 2), it can be empirically described by a two-parameter function. As an exercise, the mass-dependence of the parameters were determined on Drell-Yan events, their values and uncertainties in the  $m_W$  region were used to produce  $p_T^\ell$  pseudo-data as above, and corresponding fits to  $m_W$  were performed. The spread in  $m_W$  resulting from the uncertainty in the empirical parameters was found compatible with the above estimate.

## 5 Environmental uncertainties

### 5.1 Backgrounds

The leptonic  $W$  final states benefit from low backgrounds, mostly coming from vector boson decays; notably  $W \rightarrow \tau(\rightarrow \ell\nu\nu)\nu$  (irreducible),  $Z \rightarrow \ell\ell$  (where one lepton is not reconstructed), and  $Z \rightarrow \tau(\rightarrow \ell\nu\nu)\tau$ . QCD dijet events will, despite their large cross section, not be dominant. The backgrounds from  $t\bar{t}$  and  $W^+W^-$  events are negligible. The systematic error on  $m_W$  arises from uncertainties on the background shape and normalization in the fitting range of the  $p_T^\ell$  and  $m_T^W$  spectra.

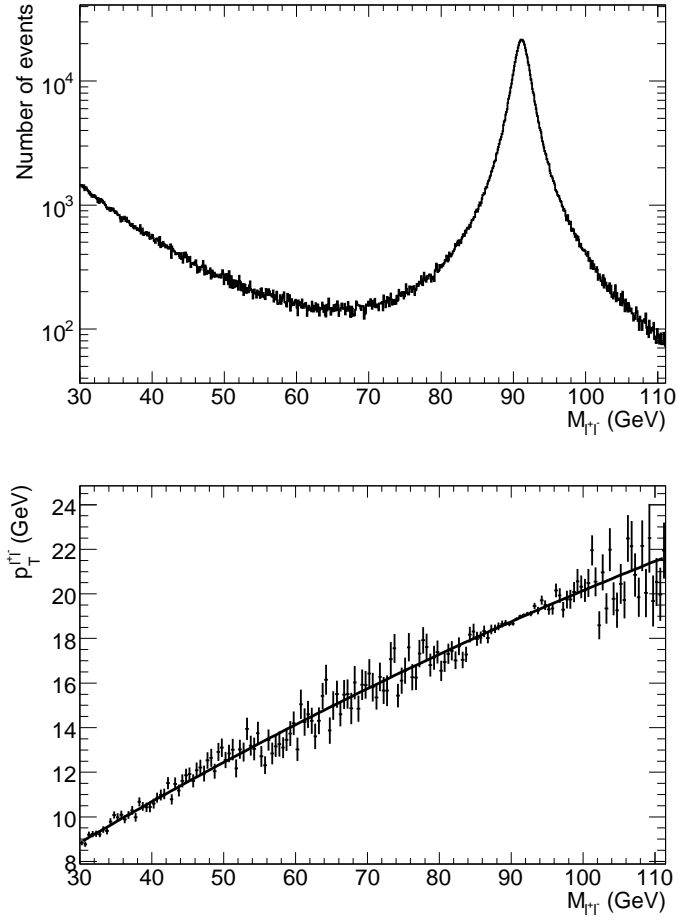


Figure 20: Top : Dilepton invariant mass spectrum, from inclusive neutral current events ( $\gamma$  and  $Z$  exchange are included). Bottom : dilepton average  $p_T$  as a function of the dilepton invariant mass. The  $W$ -mass region is strongly constrained by the lever arm provided by the  $Z$  peak and the Drell-Yan rise at low mass (note the improved precision in these regions). The points correspond to a measurement with  $10 \text{ fb}^{-1}$ .

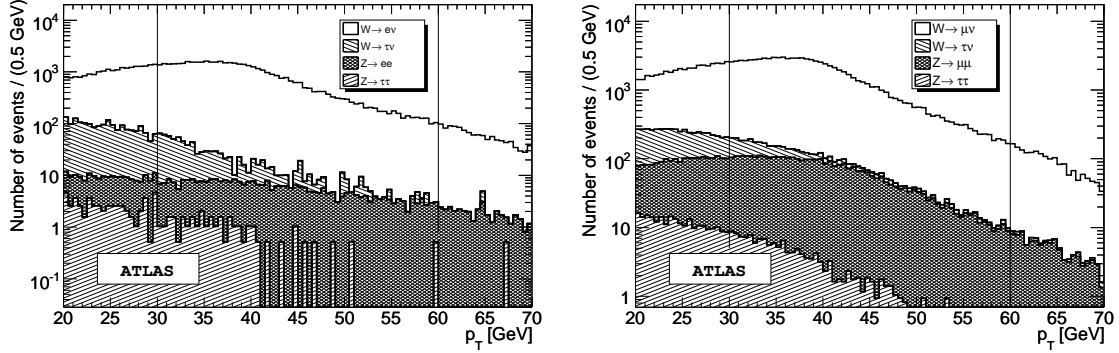


Figure 21: Signal and backgrounds in the  $p_T^\ell$  distributions, for  $W \rightarrow e\nu$  (left) and  $W \rightarrow \mu\nu$  (right). The histograms correspond, from bottom to top, to  $Z \rightarrow \tau\tau$ ,  $Z \rightarrow \ell\ell$ ,  $W \rightarrow \tau\nu$  and  $W \rightarrow \ell\nu$ .

Uncertainties on the  $W$  and  $Z$  background size, relative to the signal size, depend on cross-sections, branching fractions and acceptances. These are obtained from the PDG [28] and take into account the studies described in Section 3.2 and 4.3. Note that in contrast to the studies presented until now, the background uncertainty does not scale with statistics.

The background shapes are determined from simulation. They are essentially unaffected by variations in the production, decay, and resolution model, and play only a minor role in the overall systematic errors. For QCD background, as a separate study, both normalization and shape will have to be measured directly from the data. The  $p_T^\ell$  distributions, including signal and backgrounds, are illustrated in Figure 21.

**$W \rightarrow \tau\nu$  events:** The largest background is from  $W \rightarrow \tau\nu$  events, where the  $\tau$  decays into a lepton. This background is irreducible, as the final state is identical to the signal; however, its  $p_T^\ell$  and  $m_T^W$  are on average lower, leaving a tail into the fitting range. Though being the main background, its uncertainty is small, as only  $\tau$  decay parameters and the acceptance enter, with respective uncertainties of 1% and 2.5%.

**$Z \rightarrow \ell\ell$  events:** The second largest background is from  $Z \rightarrow \ell\ell$  events, where one lepton is either undetected or not identified. This background can be reduced using a  $Z$  veto rejecting events, where the lepton and a second isolated object (track and/or cluster) form an object with an invariant mass between 80 and 100 GeV (see Figure 22). Due to the high mass of the  $Z$  boson, the  $p_T^\ell$  distribution extends well into the fitting range. The  $m_T^W$  distribution is again at low values, due to the smallness of missing momentum. The size of this background has uncertainties from both the  $W$  to  $Z$  cross section ratio  $R_{WZ}$ , and from the acceptance/veto efficiency. It is expected to be larger for muons than for electrons, as the former cannot be vetoed for  $|\eta| > 2.7$ .



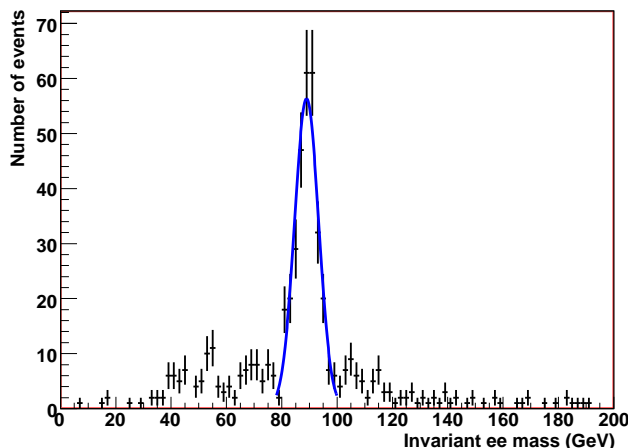


Figure 22: Distribution of invariant mass between lepton and a second isolated object (track and/or cluster) in  $Z \rightarrow \ell\ell$  events where only one lepton is identified. Events in the range 80-100 GeV are rejected.

**$Z \rightarrow \tau\tau$  events:** A small background originates from the  $Z \rightarrow \tau\tau$  process, where one  $\tau$  decays leptonically, while the other is not identified. While the cross section for such a process is small, it contains significant  $E_T^{miss}$ .

**Jet production:** The QCD background cannot be obtained reliably from simulation. It will thus have to be measured directly from data. For the Run I  $W$  mass measurement at CDF, this background could be estimated to a precision of  $\sim 50\%$  [45], limited by lepton identification performances and statistics. At ATLAS, a precision of  $\sim 10\%$  is assumed in the electron channel, where this background is expected to be significant. The assumed improvement is justified by the superior granularity and resolution of the EM calorimeter [15]. The muon final state is less contaminated by jet events, muons being measured behind all calorimetry. A specific background is however constituted by muons from hadron decays in flight. As we have no measure of the uncertainty on this background, our results implicitly assume it is small. We stress that these estimates are essentially qualitative. A realistic estimate of their impact on the measurement will only be possible with data.

**Overall impact:** We now estimate the overall impact of the backgrounds. The background shapes can be empirically described by an exponential function in the fitting range, as illustrated in Figure 23 on the example of the  $W \rightarrow \tau\nu$  background. The systematic uncertainty on  $m_W$  is then derived by varying the function parameters within their uncertainties as estimated above. The systematics uncertainty induced by the background shapes amounts to 20% of that induced by the normalizations.

The overall effect is obtained by repeating this procedure for all backgrounds. Table 3 summarizes background uncertainty and its impact on the  $W$  mass determination.

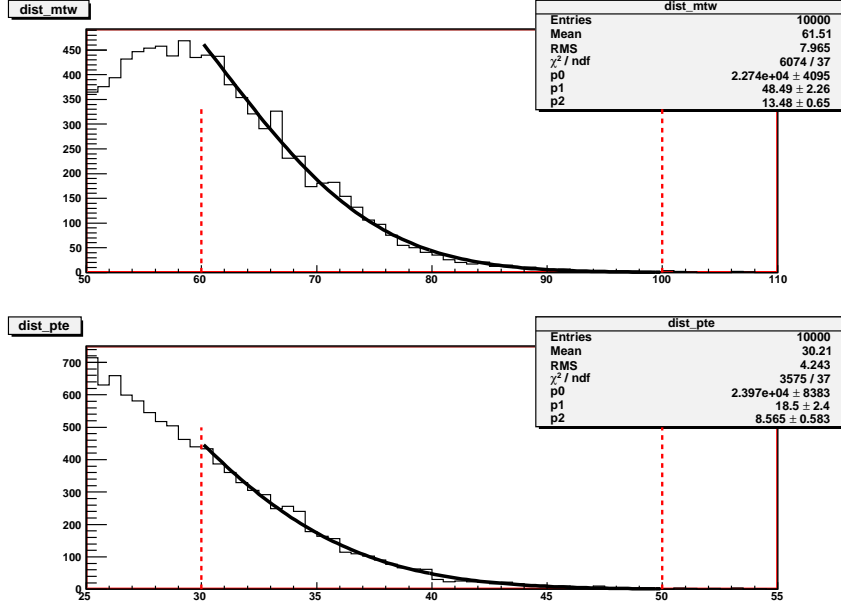


Figure 23:  $W \rightarrow \tau \nu$  background shape in the fitting range (indicated by dashed lines) for  $m_T^W$  (top) and  $p_T^\ell$  (bottom).

Background	Variable	Error	Derivative	Impact (MeV)
$W \rightarrow \tau \nu$	$m_T^W$	2.5 %	-0.5 MeV/%	1.5
	$p_T^\ell$	2.5 %	-0.7 MeV/%	2.0
$Z \rightarrow \ell(\ell)$	$m_T^W$	2.8 %	0.08 MeV/%	0.22
	$p_T^\ell$	2.8 %	0.09 MeV/%	0.26
$Z \rightarrow \tau \tau$	$m_T^W$	4.5 %	0.02 MeV/%	0.09
	$p_T^\ell$	4.5 %	0.03 MeV/%	0.14
QCD events	$m_T^W$	10 %	0.04 MeV/%	0.40
	$p_T^\ell$	10 %	0.05 MeV/%	0.50
Total	$m_T^W$			1.6
	$p_T^\ell$			2.1

Table 3: Table of backgrounds along with its uncertainty, derivative, and impact on  $m_W$ . The overall systematic uncertainty from backgrounds is about 2 MeV.

Combining the systematic errors from the backgrounds yields a total of 1.6 and 2.1 MeV for the  $m_T^W$  and  $p_T^\ell$  distributions, respectively.

## 5.2 Pileup and underlying event

The soft hadronic activity accompanying the hard process (underlying event), and the overlap with soft events produced in the same bunch crossing (pile-up) generate additional particles that contribute to the detector occupancy. In particular, the additional calorimetric energy overlaps with the electron signal and distorts the electron scale measurement.

Typically, a soft event produces about 10 particles per unit rapidity (integrated over  $\phi$ ), with average transverse momentum  $p_T \sim 500$  MeV [46,47]. An electron cluster of typical size  $\delta\eta \times \delta\phi \sim 0.1 \times 0.1$  is expected to contain about 40 MeV of hadronic background, to be subtracted from the electron signal.

In particular, the hadronic background may have a non-negligible  $Q^2$ -dependence, generating a non-universality between  $W$  and  $Z$  events. These effects are small but need to be properly accounted for when aiming at a precision on the absolute electron scale of  $\delta\alpha/\alpha \sim 2 \times 10^{-5}$ .

This aspect was not studied here, but we follow the argument of [15]. By measuring the energy flow away from any high- $p_T$  objects, as a function of  $\eta$ , independently in  $W$  and  $Z$  events, a 2% precision on the hadronic energy flow looks achievable. Such a result would bring down the size of the effect from 40 MeV to about 1 MeV.

We thus conclude that although soft hadronic interactions generate shifts in the energy measurements that are large compared to the statistical sensitivity to  $m_W$ , these shifts can be measured in the data with sufficient accuracy. The final contribution to  $\delta m_W$  is small.

This source of uncertainty affects the electron scale; the muon scale is not affected. The impact on the recoil measurement is not discussed here; this section is thus relevant for  $p_T^\ell$  based measurements.

## 5.3 Beam crossing angle

At the LHC, the proton beams are brought to collision at a crossing angle of  $142.5 \mu\text{rad}$  [48]. In terms of momentum, this translates into a  $7000 \text{ GeV} \times 142.5 \times 10^{-6} \approx 1 \text{ GeV}$  boost in the horizontal plane ( $x$ -direction), per beam proton. However, in the simulation protons collide head-on, giving rise to a systematic shift in  $p_x$  of all particles produced.

Figure 24 shows the difference in the transverse  $W$  momentum before and after taking this effect into account,  $\Delta p_x^W = p_x^W - p_x^{boost}$ , which is expected to be up to  $\Delta p_x^W = m_W \cdot 142.5 \times 10^{-6} \approx 11$  MeV. However, since the  $W$  boson line of flight has azimuthal symmetry, the impact on the  $W$  transverse momentum distribution is smaller, as most of the effect is averaged out by the rotational symmetry.

The size of the effect is estimated as usual, by including the  $p_x^{boost}$  in the pseudo-data and letting the templates unchanged. We find that the effect is smaller than 0.1 MeV.

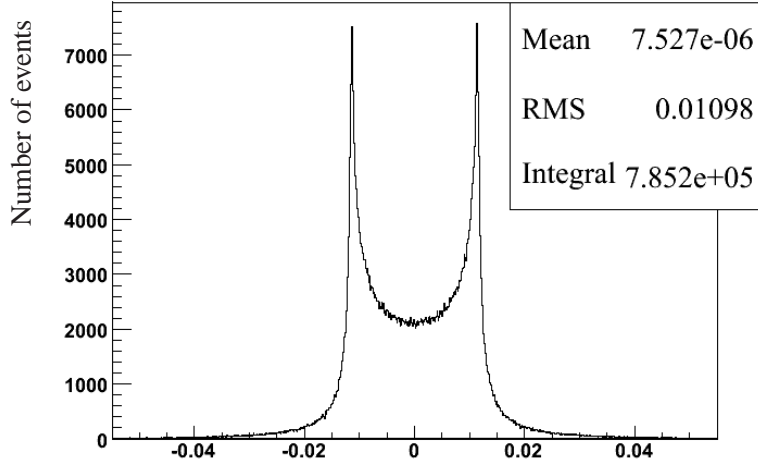


Figure 24: Distribution of difference in the transverse  $W$  momentum resulting from the boost,  $\Delta p_x^W = p_x^W - p_x^{boost}$ .

## 6 Correlations

So far, all main sources of systematic uncertainties have been investigated independently. Before we move to the combination of our results, we need to address the question whether important correlations are to be expected between the sources. It is, however, beyond the scope of this work to discuss this issue extensively, and we limit this section to the most important examples.

The uncertainty related to the absolute scale has the strongest lever arm on the determination of  $m_W$  ( $\delta m_W / \delta \alpha = 1$ ). Therefore, we investigate below whether uncertainties which affect the  $W$  mass measurement can also bias the absolute scale.

### 6.1 Absolute scale vs. lepton reconstruction efficiency

We repeat the procedure described in Section 3.1. As before,  $Z$  boson invariant mass templates are produced for different scale and resolution hypotheses, and pseudo-data with scale parameters to be determined. The impact of a  $p_T^\ell$ -dependent lepton reconstruction efficiency is assessed by assuming perfect efficiency in the templates ( $\varepsilon = 1$ ), and injecting the efficiency function discussed in Section 3.2 in the pseudo-data.

The result is displayed in Figure 25. It appears that the injected inefficiencies merely induce a reduction of statistics, and hence some loss of precision in the scale determination, but no appreciable bias: in spite of the reduction in statistics, the reference invariant mass distribution is not significantly distorted. Note that, since the efficiency is assumed perfect in the templates, and realistic in the pseudo-data, any observed bias would have been a large overestimation of the effect, representing 100% uncertainty on the effect.

### 6.2 Absolute scale vs. PDFs

Similarly as above, and also as in Section 4.3.1, we compare  $Z$  boson mass templates produced with the CTEQ6.1 central set to pseudo-data produced with the 40 uncertainty sets.

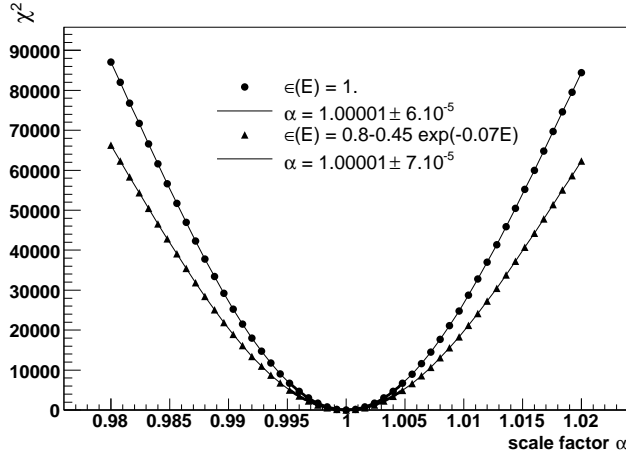


Figure 25: Scale determination using  $Z$  mass templates assuming perfect identification efficiency. Inner parabola: perfect efficiency is also assumed in the pseudo-data; outer parabola: the pseudo-data incorporate a  $p_T$ -dependent efficiency.

The results of the 40 fits are displayed in Figure 26, in the form of biases with respect to position of the mass peak obtained in the templates. The CTEQ6.1 uncertainty sets induce typical biases of  $\sim 0.5$  MeV with respect to the central value. Summing over all uncertainty sets gives a total scale uncertainty of about 2.5 MeV. This translates into  $\delta m_W \sim 2.2$  MeV.

In other words, with current knowledge, the PDF uncertainties induce a direct systematic uncertainty of about 25 MeV *via* distortions of the  $W$  distributions (cf. Section 4.3.1), and an indirect uncertainty of 2.2 MeV *via* distortions of the  $Z$  lineshape, propagating to the absolute scale determination.

Hence, the conclusions of Section 4.3.1 are essentially unchanged. Using measurements of the  $Z$  boson distributions, the PDF induced systematic uncertainty should drop to about 1 MeV.

### 6.3 Absolute scale vs. QED corrections

QED corrections affect the determination of the absolute scale in two ways. First, as was mentioned in Section 4.2, the observed  $W$  and  $Z$  decay lepton spectra are strongly affected by photon emission. This effect needs to be taken into account properly when producing the  $Z$  mass templates.

In muon final states, the theoretical distributions are based on the final muons, after simulation of the QED photon emissions. Final state electrons cannot be separated experimentally from the mostly collinear photons. Hence, the simulation needs to reproduce this recombination precisely. This demands precise theoretical control of the photon distributions, an aspect which seems under sufficient control (cf. Section 4.2). Likewise, a precise description of the detector geometry and EMC shower development in the simulation are needed to properly simulate the fraction of photon energy recombined in a given electron cluster.

Secondly, as a consequence of the above, the absolute scale extracted from  $Z$  events actually corre-

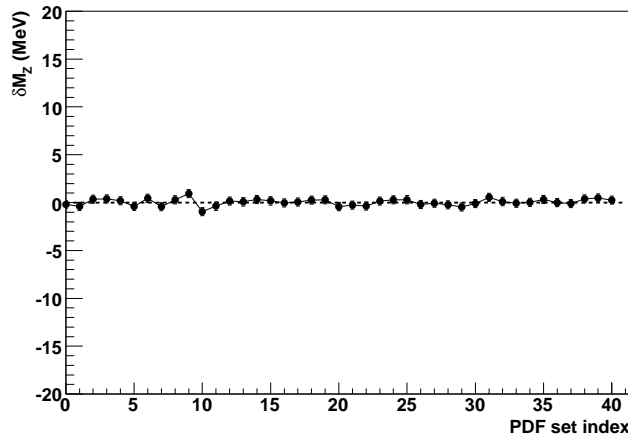


Figure 26: Bias on  $m_Z$  obtained when varying the proton PDFs within their uncertainties. Each point on the abscissa corresponds to a given PDF set: set 0 is the best fit, and gives 0 bias by definition; sets 1-40 are the uncertainty sets, each inducing a given bias on  $m_Z$ . The total uncertainty is given by the quadratic sum of the biases, giving  $\delta m_Z \sim 2.5$  MeV.

sponds to a mixture of photons and electrons. In ATLAS, the EMC response to electrons and photons is different by about 1%, an effect coming from calorimeter geometry (because their showers develop differently, electrons and photons of a given energy do not “feel” the same sampling fraction) and from the passive material in front of the EMC, which causes early showers or conversions, with different probabilities for both particle types [49]. It is thus important to know whether  $W$  and  $Z$  behave similarly in this respect, and if any difference is well understood theoretically.

As is shown in Figure 27, the electron energy fraction in EM clusters differs by about 0.6% between  $W$  and  $Z$  events, meaning that the energy scale measured in  $Z$  events needs to be corrected by a factor  $1\% \times 0.6\% = 6 \times 10^{-5}$ . Failing to take this factor into account would induce a bias of  $\sim 5$  MeV on the  $m_W$  fit. However, Figure 27 also shows a good stability of the theoretical prediction. Hence, although this correction is not negligible, it does not carry a significant uncertainty.

## 7 Impact on the $W$ mass measurement

We summarize below our main results. Table 4 recalls the main systematic contributions to the  $p_T^\ell$ - and  $m_T^W$ -based  $m_W$  measurement, with  $10 \text{ fb}^{-1}$  of data. In both tables, numbers are given for the electron and muon channels separately when applicable.

The major difficulty is, as expected, the determination of the absolute energy scale of the final state leptons and the hadronic recoil. The analysis of the  $Z$  peak however allows to strongly constrain the lepton scale uncertainty. The analysis is non trivial, because in addition to the  $Z$  mass parameters, many other effects enter the theoretical description of the lineshape; most notably, QED radiation. Although the effect is large, the theoretical understanding is adequate, as the LEP1  $Z$  mass measurement indicates. The  $Z$  mass measurement relies on an analytical formulation of the inclusive radiation

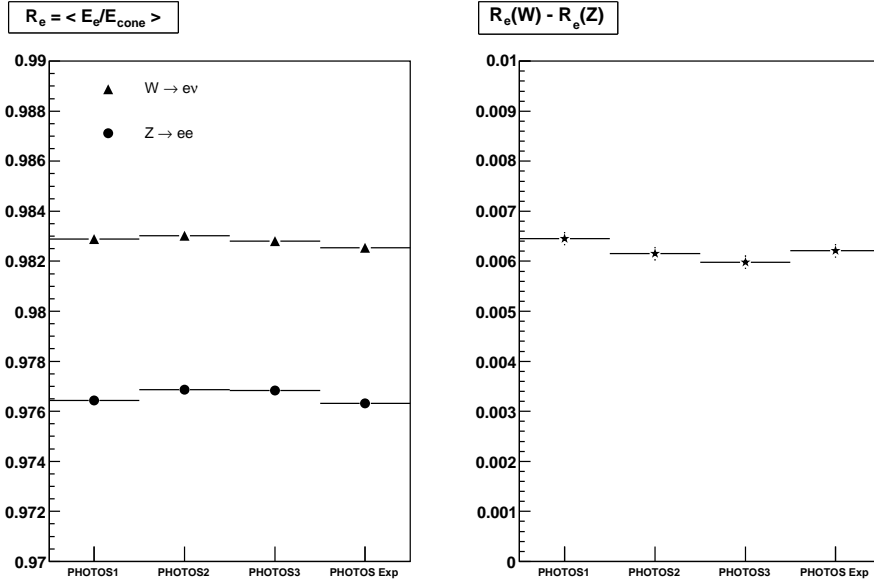


Figure 27: For electron final states in  $W$  and  $Z$  events, the energy fraction  $R_e$  deposited by electrons in reconstructed electromagnetic clusters ( $1-R_e$  is photon energy), for various PHOTOS settings (see Section 4.2).

spectrum; the  $W$  mass measurement at the LHC however requires a complete Monte-Carlo implementation, providing an exclusive description of the final state at the same level of precision. Such tools are critically needed in the context of this measurement.

The analysis of the transverse mass requires in addition a precise calibration of the hadronic recoil using  $Z$  events, and an unbiased transport of the calibration to  $W$  events. Such an algorithm is not discussed here; the corresponding systematic uncertainty assumed here is a compromise between the high statistical sensitivity of the in situ calibration in ATLAS, and the actual result recently obtained at the Tevatron [10].

The electron channel appears somewhat more difficult than the muon channel. The first reason is the  $p_T$ -dependent electron identification efficiency, which distorts the Jacobian distributions; this effect is essentially absent in the muon channel. The second reason is again related to QED radiation: since the muons do not recombine with the emitted photons, the description of the effect is purely theoretical. In the case of electrons, a large fraction of the radiated energy is included in the electron cluster. Determining this fraction requires a precise description of the detector geometry and reliable simulation of EM showers.

We estimate that uncertainties related to the description of the  $y^W$  and  $p_T^W$  distributions will be small once the  $Z$  differential cross-section will have been measured. As discussed in Sections 4.3.1 and 4.3.2, this result relies on two assumptions. The first assumption concerns the light quark flavour and charge symmetry in the low- $x$ , high- $Q^2$  proton. We estimated that relaxing these hypotheses within bounds allowed by the existing data is unlikely to invalidate our result. Another assumption is that the non-



perturbative mechanisms controlling the  $p_T^W$  and  $p_T^Z$  distributions remain essentially universal, although heavy flavour contributions to  $W$  and  $Z$  production are different. The effect of heavy flavours on the  $p_T^W$  distribution has been studied [50], but a study comparing these effects on  $W$  and  $Z$  production is currently lacking. The largest remaining systematic comes from the modeling of  $p_T^W$ , in the  $p_T^\ell$ -based measurement, contributing a 3 MeV uncertainty. The  $m_T^W$ -based measurement is more stable in this respect, but suffers additional experimental complications related to the experimental control of the  $E_T^{miss}$  reconstruction.

Backgrounds contribute an uncertainty  $\delta m_W \sim 2$  MeV. Of all components, the background from jet production is the least well known, but its contribution is expected to be small. We did not investigate the possible impact of cosmic rays and hadron decays in flight, which occur in the muon channels, but Tevatron experience indicates the impact is small.

All in all, a total uncertainty of about 7 MeV can be achieved, in each channel, using either the  $p_T^\ell$  or the  $m_T^W$  method, with the equivalent of  $10 \text{ fb}^{-1}$  of data. Most sources of systematic uncertainty seem to scale with the accumulated  $Z$  statistics; notable exceptions are backgrounds, QED radiative corrections and the underlying event. Their contribution to  $\delta m_W$  is however subdominant. Combining channels, and allowing for more data, we can therefore expect further improvement.

Let us briefly compare our results with the recent prospects presented by the CMS Collaboration [14]. We base our comparison on the  $p_T^\ell$ -based  $m_W$  measurement and  $10 \text{ fb}^{-1}$  of data. CMS claims 2 MeV from the absolute scale, agreeing with our average scale result of Section 3.1.1. A simplified treatment of non-linearities leaves a systematic uncertainty of 10 MeV, and the assumed 8% relative knowledge on the resolution contributes 5 MeV; these numbers can be compared to the 4 MeV we obtain in Section 3.1.2. We include a discussion of the reconstruction efficiency uncertainty, which is omitted in [14]. On the theoretical side, the present note and Reference [14] agree on the initial uncertainties related to PDFs and the description of the  $W$  transverse momentum distribution. Our improvements in this respect rely on an analysis of the constraints provided by the analysis of the  $Z$  boson differential cross-section at the LHC. Finally, we claim a statistical sensitivity of about 2 MeV, compared to 15 MeV in [14]. This is explained by CMS choosing to base the  $W$  templates on measured  $Z$  events (*via* the scaled observable method, or scaling the kinematics event by event), thus paying for the smaller  $Z$  boson production rate. Such a procedure is in principle justified by the reduction of other systematic uncertainties, but as we saw throughout this paper this does not seem to be a worthy trade.

## 8 Conclusions and perspectives

We investigated the most important systematic uncertainties affecting the  $W$  mass determination at the LHC, and found that the analysis of  $Z$  production constrains the systematic uncertainties to a total of about 7 MeV per channel, exploiting  $10 \text{ fb}^{-1}$  of data. Combining independent measurements may bring further improvement.

Among all investigated sources of systematic uncertainty, two items in particular rely on assumptions. The first one concerns the treatment of QED radiation. We argued that the theory is under very good control, having notably allowed a very precise  $Z$  mass measurement at LEP1, where QED effects are large, but the uncertainties finally have an almost negligible contribution. To preserve this situation at the LHC, the  $m_W$  measurement requires QED simulation tools providing the same level of accuracy.

Source	Effect	$\partial m_W / \partial_{rel} \alpha$ (MeV/%)	$\delta_{rel} \alpha$ (%)	$\delta m_W$ (MeV)
Prod. Model	$W$ width	1.2	0.4	0.5
	$y^W$ distribution	—	—	1
	$p_T^W$ distribution	—	—	3
	QED radiation	—	—	<1 (*)
Lepton measurement	Scale & lin.	800	0.005	4
	Resolution	1	1.0	1
	Efficiency	—	—	4.5 (e) ; <1 ( $\mu$ )
Recoil measurement	Scale	—	—	—
	Resolution	—	—	—
Backgrounds	$W \rightarrow \tau \nu$	0.15	2.5	2.0
	$Z \rightarrow \ell(\ell)$	0.08	2.8	0.3
	$Z \rightarrow \tau \tau$	0.03	4.5	0.1
	Jet events	0.05	10	0.5
Pile-up and U.E				<1 (e); $\sim 0(\mu)$
Beam crossing angle				<0.1
Total ( $p_T^\ell$ )				$\sim 7$ (e); $6(\mu)$

Source	Effect	$\partial m_W / \partial_{rel} \alpha$ (MeV/%)	$\delta_{rel} \alpha$ (%)	$\delta m_W$ (MeV)
Prod. Model	$W$ width	3.2	0.4	1.3
	$y^W$ distribution	—	—	1
	$p_T^W$ distribution	—	—	1
	QED radiation	—	—	<1 (*)
Lepton measurement	Scale & lin.	800	0.005	4
	Resolution	1	1.0	1
	Efficiency	—	—	4.5 (e) ; <1 ( $\mu$ )
Recoil measurement	Scale	-200	—	—
	Resolution	-25	—	—
	Combined	—	—	5 (**)
Backgrounds	$W \rightarrow \tau \nu$	0.11	2.5	1.5
	$Z \rightarrow \ell(\ell)$	-0.01	2.8	0.2
	$Z \rightarrow \tau \tau$	0.01	4.5	0.1
	Jet events	0.04	10	0.4
Pile-up and U.E				<1 (e); $\sim 0(\mu)$
Beam crossing angle				<0.1
Total ( $m_T^W$ )				$\sim 8$ (e); $7(\mu)$

Table 4: Breakdown of systematic uncertainties affecting the  $m_W$  measurement, when using the  $p_T^\ell$  distribution (top) and the  $m_T^W$  distribution (bottom). The projected values of  $\delta_{rel} \alpha$  are given for a single channel and assume an integrated luminosity of  $10 \text{ fb}^{-1}$ . The QED induced uncertainty (\*) is realistic given the precision claimed for the  $Z$  boson mass measurement at LEP1, but assumes that the needed theoretical tools will be implemented in time for the measurement. The recoil measurement uncertainty (\*\*) has not explicitly been quantified here, but is conservatively extrapolated from recent Tevatron experience. See text for discussion.

The second assumption concerns the effect of the light and heavy flavours in the proton. Releasing the light flavour symmetry assumption in use in the current global QCD fits will cause a decorrelation between  $W$  and  $Z$  production at the LHC. This decorrelation can be expected to be small, but will have to be measured at the LHC, notably using the rapidity-dependent  $W$  charge asymmetry and the study of associated  $W/Z$  + charm production. Similarly, heavy flavour PDFs generate some decorrelation. This decorrelation was verified to be small in the  $y^W$  and  $y^Z$  distributions, and the same was assumed true for the  $p_T^W$  and  $p_T^Z$  distributions. To verify this assumption requires a theoretical study comparing the heavy flavours influence on soft gluon resummation in  $W$  and  $Z$  events.

A number of sources have not been studied explicitly, notably the recoil measurement, affecting the  $m_T^W$  distribution; the underlying event, affecting the electron energy scale; and  $W$  polarization effects, affecting the leptonic angular distributions. Other sources, like backgrounds from jets, cosmic muons, or induced by the machine can only be studied reliably using real data. We believe these mechanisms can be brought under sufficient control, on the time scale of the LHC measurement of  $m_W$ .

The results presented here have only exploited  $Z$  boson measurements. Many other calibration processes exist, that give additional constraints on the detector performance and on the physics mechanisms influencing  $W$  production. While first providing a way to verify the robustness of the  $Z$ -based calibrations, these processes can help to reduce the uncertainties further in the case of consistent results. We reserve these refinements to the analysis of the forthcoming LHC data.

## 9 Acknowledgements

This work has continuously benefitted from feedback, suggestions and discussions. Within the ATLAS Collaboration, we would like to thank Lucia di Ciaccio, Amanda Cooper-Sarkar, Fares Djama, Daniel Froidevaux, Joey Huston, Karl Jakobs, Max Klein, Ashutosh Kotwal, Witek Krasny, Tom LeCompte, Dan Levin, Guillaume Unal, and many others. We are also grateful to Philippe Charpentier and Olivier Schneider from LHCb. From the theoretical community, we acknowledge discussions with Stefan Berge, Walter Giele, Staszek Jadach, Pavel Nadolsky, Fred Olness, Fulvio Piccinini, and Zbyszek Was.

## References

- [1] M. Awramik, M. Czakon, A. Freitas and G. Weiglein, Phys. Rev. **D69**, 053006 (2004).
- [2] M. Awramik, M. Czakon and A. Freitas, JHEP **11**, 48 (2006).
- [3] ALEPH, DELPHI, L3, OPAL and SLD Collaborations, Phys. Rept. **427**, 257 (2006).
- [4] D0 Collaboration, Phys. Rev. Lett **74**, 2632 (1995).
- [5] CDF Collaboration, Phys. Rev. Lett. **74**, 2626 (1995).
- [6] ALEPH, DELPHI, L3 and OPAL Collaborations, hep-ex/0612034.
- [7] S. Heinemeyer, W. Hollik and G. Weiglein, Phys. Rept. **425**, 265 (2006).

- [8] UA2 Collaboration, Phys. Lett. **B276**, 354 (1992).
- [9] CDF and D0 Collaborations, Phys. Rev. **D70**, 092008 (2004).
- [10] CDF Collaboration, Phys. Rev. Lett. **99**, 151801 (2007).
- [11] K. Melnikov and F. Petriello, Phys. Rev. **D74**, 114017 (2006).
- [12] ATLAS Collaboration, CERN/LHCC/99-15.
- [13] S. Haywood et al., hep-ph/0003275.
- [14] V. Buge et al., J. Phys. **G34**, N193 (2007).
- [15] ATLAS Collaboration, CERN/LHCC/99-14.
- [16] T. Sjostrand, S. Mrenna and P. Skands, JHEP **05**, 026 (2006).
- [17] P. Golonka and Z. Was, Eur. Phys. J. **C45**, 97 (2006).
- [18] C. Balazs and C. P. Yuan, Phys. Rev. **D56**, 5558 (1997).
- [19] D. Froidevaux, L. Poggioli and E. Richter-Was, ATL-PHYS-98-131.
- [20] A. Rimoldi et al., *ATLAS detector simulation: Status and outlook*, Prepared for 9th ICATPP Conference on Astroparticle, Particle, Space Physics, Detectors and Medical Physics Applications, Villa Erba, Como, Italy, 17-21 Oct 2005.
- [21] ATLAS Collaboration, *The ATLAS Experiment at the CERN Large Hadron Collider*, submitted to JINST (2008).
- [22] E. Mirkes and J. Ohnemus, Phys. Rev. **D50**, 5692 (1994).
- [23] D0 Collaboration, Phys. Rev. **D61**, 032004 (2000).
- [24] S. Berge, P. Nadolsky, F. Olness and C. P. Yuan, Phys. Rev. **D72**, 033015 (2005).
- [25] C. M. Carloni Calame, G. Montagna, O. Nicrosini and M. Treccani, Phys. Rev. **D69**, 037301 (2004).
- [26] N. Besson and M. Boonekamp, ATL-PHYS-PUB-2006-007.
- [27] ATLAS Electromagnetic Barrel Calorimeter Collaboration, Nucl. Instrum. Meth. **A568**, 601 (2006).
- [28] Particle Data Group, J. Phys. **G33**, 1 (2006).
- [29] CDF and D0 Collaborations, Phys. Rev. **D70**, 092008 (2004).
- [30] CDF Collaboration, Phys. Rev. Lett. **100**, 071801 (2008).
- [31] D. R. Yennie, S. C. Frautschi and H. Suura, Ann. Phys. **13**, 379 (1961).
- [32] G. Nanava and Z. Was, hep-ph/0607019.
- [33] J. Pumplin et al., JHEP **07**, 012 (2002).

- [34] P. M. Nadolsky, AIP Conf. Proc. **753**, 158 (2005).
- [35] NA51 Collaboration, Phys. Lett. **B332**, 244 (1994).
- [36] FNAL E866/NuSea Collaboration, Phys. Rev. **D64**, 052002 (2001).
- [37] NuTeV Collaboration, Phys. Rev. **D65**, 111103 (2002).
- [38] V. Barone, C. Pascaud and F. Zomer, Eur. Phys. J. **C12**, 243 (2000).
- [39] F. Olness et al., Eur. Phys. J. **C40**, 145 (2005).
- [40] A. D. Martin, R. G. Roberts, W. J. Stirling and R. S. Thorne, Eur. Phys. J. **C23**, 73 (2002).
- [41] S. Alekhin et al., *HERA and the LHC - A workshop on the implications of HERA for LHC physics: Proceedings Part A*, (2005), hep-ph/0601012.
- [42] J. Pumplin et al., JHEP **02**, 053 (2007).
- [43] J. C. Collins, D. E. Soper and G. Sterman, Nucl. Phys. **B250**, 199 (1985).
- [44] G. Miu and T. Sjostrand, Phys. Lett. **B449**, 313 (1999).
- [45] A. S. Gordon, *Measurement of the W boson mass with the Collider Detector at Fermilab*, FERMILAB-THESIS-1998-10.
- [46] A. Moraes et al., ATL-PHYS-PUB-2005-007.
- [47] A. Moraes et al., ATL-PHYS-PUB-2005-015.
- [48] O. S. Bruning, W. Herr and R. Ostojic, LHC-Project-Report-315.
- [49] ATLAS Collaboration, CERN/LHCC/96-41.
- [50] S. Berge, P. M. Nadolsky and F. Olness, Phys. Rev. **D73**, 013002 (2006).